Article

Cell Reports

The CoQH2/CoQ Ratio Serves as a Sensor of Respiratory Chain Efficiency

Graphical Abstract

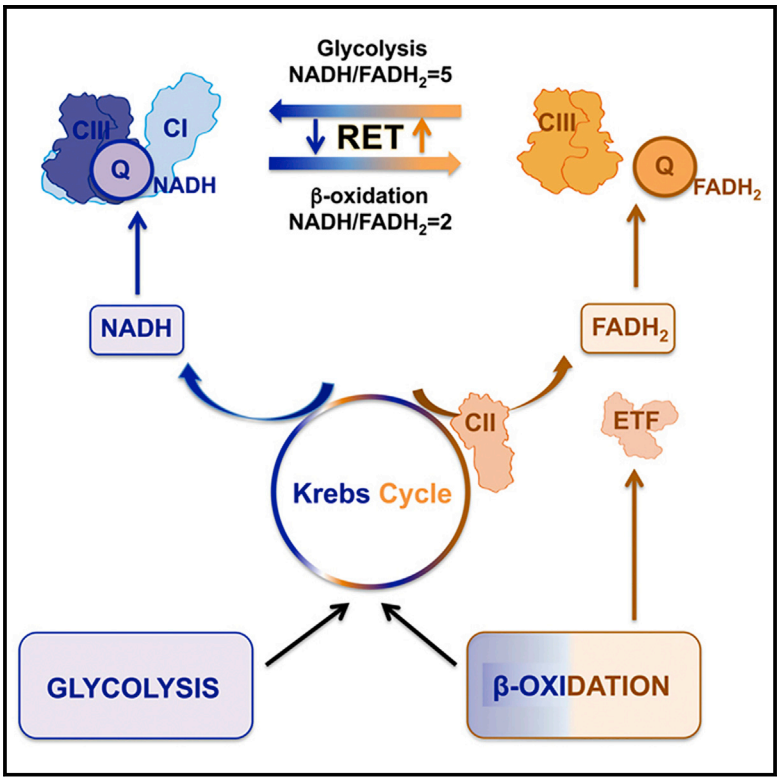

Authors

Adela Guarás, Ester Perales-Clemente, Enrique Calvo, ..., Plácido Navas, Jesús Vazquez, Jose A. Enríquez

Correspondence

jaenriquez@cnic.es

In Brief

Guarás et al. show how the mitochondrial electron transport chain (mtETC) is optimized to better oxidize different nutrients or fuels using the reducing status of ubiquinone as a metabolic sensor and ROS generated by complex I by reverse electron transport as an executor.

Highlights

- High $CoQH_2$/CoQ ratio induces reverse electron transport under physiological conditions
- RET-generated ROS induces partial complex I degradation
- Increase in the CIII fraction detached of CI optimizes mETC to consume fatty acids
- The $CoQH_2$/CoQ ratio serves as a sensor of respiratory chain efficiency

Guarás et al., 2016, Cell Reports *15*, 197–209
April 5, 2016
http://dx.doi.org/10.1016/j.celrep.2016.03.009

Cell Reports
Article

The CoQH2/CoQ Ratio Serves as a Sensor of Respiratory Chain Efficiency

Adela Guarás,[1] Ester Perales-Clemente,[1] Enrique Calvo,[2] Rebeca Acín-Pérez,[1] Marta Loureiro-Lopez,[2] Claire Pujol,[3,4] Isabel Martínez-Carrascoso,[1] Estefanía Nuñez,[2] Fernando García-Marqués,[2] María Angeles Rodríguez-Hernández,[5,6] Ana Cortés,[5,6] Francisca Diaz,[7] Acisclo Pérez-Martos,[9] Carlos T. Moraes,[7,8] Patricio Fernández-Silva,[9] Aleksandra Trifunovic,[3,4] Plácido Navas,[5,6] Jesús Vazquez,[2] and Jose A. Enríquez[1,9,*]
[1]Departamento de Desarrollo y Reparación Cardiovascular
[2]Laboratorio de Proteómica Cardiovascular
Centro Nacional de Investigaciones Cardiovasculares Carlos III, Madrid 28029, Spain
[3]Cologne Excellence Cluster on Cellular Stress Responses in Aging-Associated Diseases (CECAD)
[4]Institute for Mitochondrial Diseases and Aging, Medical Faculty
University of Cologne, 50931 Cologne, Germany
[5]Centro Andaluz de Biología del Desarrollo, Universidad Pablo de Olavide-CSIC, Sevilla 41013, Spain
[6]Centro de Investigación Biomédica en Red de Enfermedades Raras, ISCIII, Sevilla 41013, Spain
[7]Department of Neurology, Miller School of Medicine, University of Miami, Miami, FL 33136, USA
[8]Department of Cell Biology and Anatomy, Miller School of Medicine, University of Miami, Miami, FL 33136, USA
[9]Departamento de Bioquímica y Biología Molecular y Celular, Facultad de Ciencias, Universidad de Zaragoza, Zaragoza 50009, Spain
*Correspondence: jaenriquez@cnic.es
http://dx.doi.org/10.1016/j.celrep.2016.03.009

SUMMARY

Electrons feed into the mitochondrial electron transport chain (mETC) from NAD- or FAD-dependent enzymes. A shift from glucose to fatty acids increases electron flux through FAD, which can saturate the oxidation capacity of the dedicated coenzyme Q (CoQ) pool and result in the generation of reactive oxygen species. To prevent this, the mETC superstructure can be reconfigured through the degradation of respiratory complex I, liberating associated complex III to increase electron flux via FAD at the expense of NAD. Here, we demonstrate that this adaptation is driven by the ratio of reduced to oxidized CoQ. Saturation of CoQ oxidation capacity induces reverse electron transport from reduced CoQ to complex I, and the resulting local generation of superoxide oxidizes specific complex I proteins, triggering their degradation and the disintegration of the complex. Thus, CoQ redox status acts as a metabolic sensor that fine-tunes mETC configuration in order to match the prevailing substrate profile.

INTRODUCTION

The mitochondrial electron transport chain (mETC), composed of four multi-subunit complexes (complex I [CI]–complex IV [CIV]) and two electron carriers (coenzyme Q [CoQ, or ubiquinone] and cytochrome *c* [cyt *c*]), generates a transmembrane proton gradient that drives ATP synthesis by complex V (CV; ATP synthase). Freely moving respiratory complexes and mobile carriers co-exist in the inner mitochondrial membrane with larger structures called respiratory supercomplexes (SCs) (Acín-Pérez et al., 2008; Enríquez, 2016). Most CI occurs in SCs with CIII, with or without CIV (CI+CIII+CIV, known as the respirasome, and CI+CIII) (Schägger and Pfeiffer, 2000). According to the Lapuente-Brun proposal (Lapuente-Brun et al., 2013), the dynamic organization into SCs creates two functional CIII populations, defined by association or non-association with CI. CI-bound CIII predominantly receives electrons from NADH ($CIII_{NADH}$), and non-CI-bound CIII ($CIII_{FAD}$) predominantly receives electrons from FAD-dependent enzymes (most commonly, CII). The mETC can fork to three forms of CIV, one interacting with CI+CIII (in the respirasome) to receive electrons from NADH (CIV_{NADH}), another interacting with non-CI-associated CIII to receive electrons from FAD (CIV_{FAD}), and a third population of free CIV able to receive electrons from CI+CIII and free CIII (CIV_{both}). CI+CIII and CIII+CIV interactions also define functional pools of CoQ and cyt *c* for carrying electrons from NADH or FAD electrons (Lapuente-Brun et al., 2013).

The CI-CIII interaction is preferential, and the amount of CI determines how much CIII is available to $FADH_2$ or NADH electrons. The proportion of electrons feeding into the mETC from NADH and $FADH_2$ varies with the carbon source. Oxidative metabolism of one molecule of glucose generates ten NADH and two $FADH_2$ electrons, a NADH:$FADH_2$ electron ratio of 5; but for a typical fatty acid (FA) like palmitate, this ratio falls to 2 (Speijer, 2011). Reorganization of the mETC superstructure in response to a substrate shift from glucose to FA was confirmed by comparing fed and starved mice. When electron flux from FAD overwhelms the oxidation capacity of CoQ_{FAD}, CI is degraded, releasing CIII from CI-containing complexes to receive FAD-derived electrons (Lapuente-Brun et al., 2013). Failure to adapt induces the generation of harmful reactive oxygen species (ROS) (Speijer, 2011). The molecular mechanism to match the mETC configuration to the relative availability of NADH and $FADH_2$ electrons is not known.

Here, by comparing cells in which CI degradation is exacerbated due to deficiency in CIII, CIV, or cyt *c* (Acín-Pérez et al.,

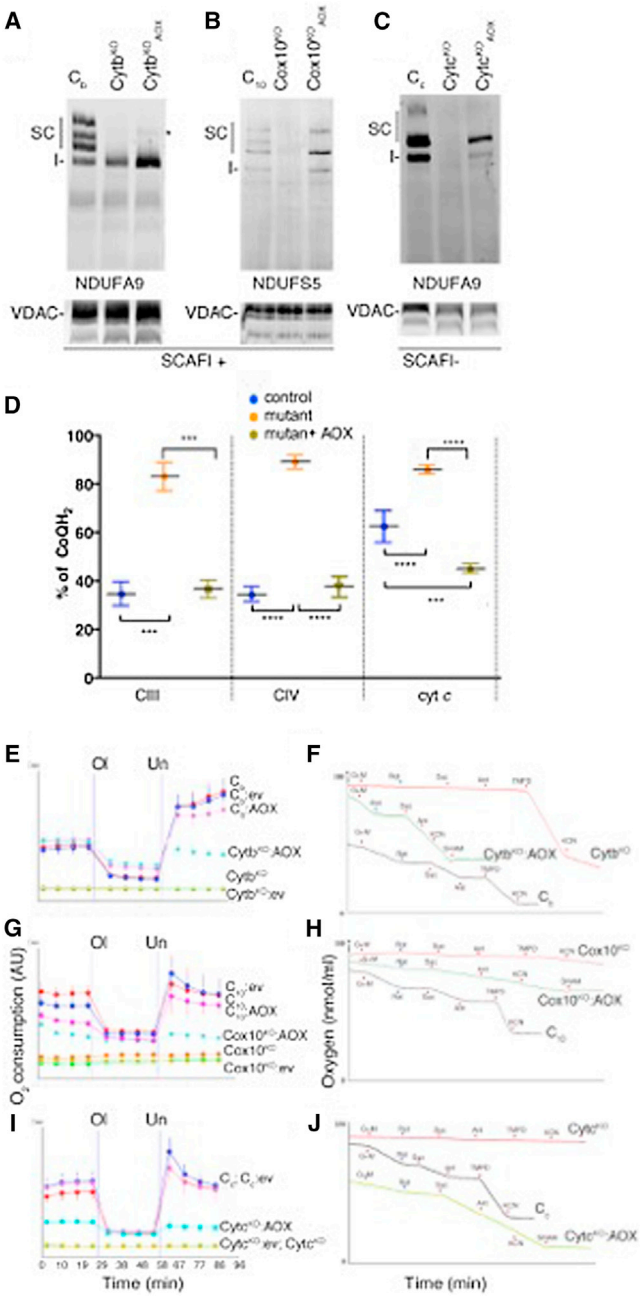

Figure 1. AOX Expression Restores Respiration in the Absence of CIII, CIV, or cyt *c*

(A–C) Detection of complexes and SCs in digitonin-solubilized mitochondria by western blot with the indicated antibodies against the CI component Ndufa9; VDAC (voltage-dependent anion channel protein) was used as a loading control. (A) Cb (isogenic control), Cytb^{KO} (lacking CIII), and Cytb^{KO}AOX cells. Star indicates a new, slow-migrating band containing CI but no other respiratory complex. (B) C_{10} (isogenic control), Cox10^{KO} (lacking CIV), and Cox10^{KO}AOX cells. (C) Cc (isogenic control), Cytc^{KO} (lacking cyt *c*), and Cytc^{KO}AOX cells.

(D) Estimated percent $CoQH_2$ in mutant cells versus isogenic controls and the effect of AOX expression. Data are mean ± SD; n = 3 to 6.

Statistical differences assessed by ANOVA ($p < 0.0001$) and Tukey's multiple comparisons test. ***$p < 0.001$; ****$p < 0.0001$ by one-way ANOVA Fisher's LSD multiple comparisons test.

2004; Diaz et al., 2006; Vempati et al., 2009), we demonstrate that CI is degraded when reduced ubiquinone (or $CoQH_2$) accumulates in the presence of oxygen. The resulting reverse electron transport (RET) generates superoxide, which oxidizes critical CI proteins, inducing their degradation. Finally, we show in vivo that modulation of $FADH_2$ electron flux to CoQ acts as a metabolic sensor, allowing mitochondria to rebalance the relative proportions of respiratory complexes to accommodate variable electron flux ratios from NADH and $FADH_2$.

RESULTS

CI Is Degraded in the Absence of CIII, CIV, or cyt *c*

To investigate the mechanism controlling the degradation of mitochondrial CI, we exploited the instability of CI assembled in cultured cells lacking CIII, CIV, or cyt *c* (Acín-Pérez et al., 2004, 2008; Diaz et al., 2006; Vempati et al., 2009). Most CI occurs in stable association with CIII (Acín-Pérez et al., 2008; Schägger and Pfeiffer, 2000), and we proposed elsewhere that this interaction stabilizes CI (Acín-Pérez et al., 2004). The steady-state level of fully assembled complexes was assessed by blue native gel electrophoresis (BNGE) followed by western blot. As reported elsewhere, in Cytb^{KO} cells, which do not assemble CIII, CI is assembled but is unstable and rapidly degraded (Acín-Pérez et al., 2004) (Figure 1A). For unknown reasons, the amount of free CI remaining in the steady state in Cytb^{KO} cells, though below the level in isogenic control cells (Cb), has increased over the years in culture. CI becomes unstable in cells lacking cox10 (Cox10^{KO}), which are unable to assemble CIV (Diaz et al., 2006) (Figure 1B) and in cells lacking cyt *c* (Cytc^{KO}), which also do not assemble CIV (Vempati et al., 2009) (Figure 1C). It should be noted that Cytc^{KO} cells and isogenic control cells (Cc) cannot incorporate CIV into SCs because they are derived from C57BL/6J mice, which harbor a mutation in SCAFI, the assembly factor required for CIII and CIV association (Lapuente-Brun et al., 2013).

Alternative Oxidase Stabilizes CI in the Absence of CIII, CIV, or cyt *c*

The primary consequence for cells of the lack of CIII, cyt *c*, or CIV is blockade of $CoQH_2$ oxidation (Figure 1D), stalling all CoQ-dependent enzymes. As a result, NADH oxidation by CI (from the matrix) and G3PDH (from the cytoplasm) is blocked, the tricarboxylic acid (TCA) cycle cannot progress from succinate to fumarate, and β-oxidation is stopped. This imbalance could trigger signaling routes to induce CI degradation. To gain knowledge about the molecular control of CI degradation, we first investigated the link between CI degradation and CoQ redox status. We inquired whether reducing $CoQH_2$ accumulation affected CI stability by expressing the alternative oxidase

(E–J) In (E), (G), and (I), oxygen consumption rates in the indicated cell lines are shown. Vertical lines mark the addition of oligomycin (Ol) or uncoupler (Un). In (F), (H), and (J), polarograph traces show O_2 consumption (nanomoles per milliliter) by the indicated cell lines. Arrowheads mark addition of the following agents: G+M, glutamate plus malate; Rot, rotenone; Suc, succinate; Ant, antimycin A; TMPD, N,N,N′,N′-tetramethyl-p-phenylenediamine; KCN, potassium cyanide; SHAM, salicylhydroxamic acid. C_b, C_{10}, and C_c, isogenic control cells. ev, empty vector.

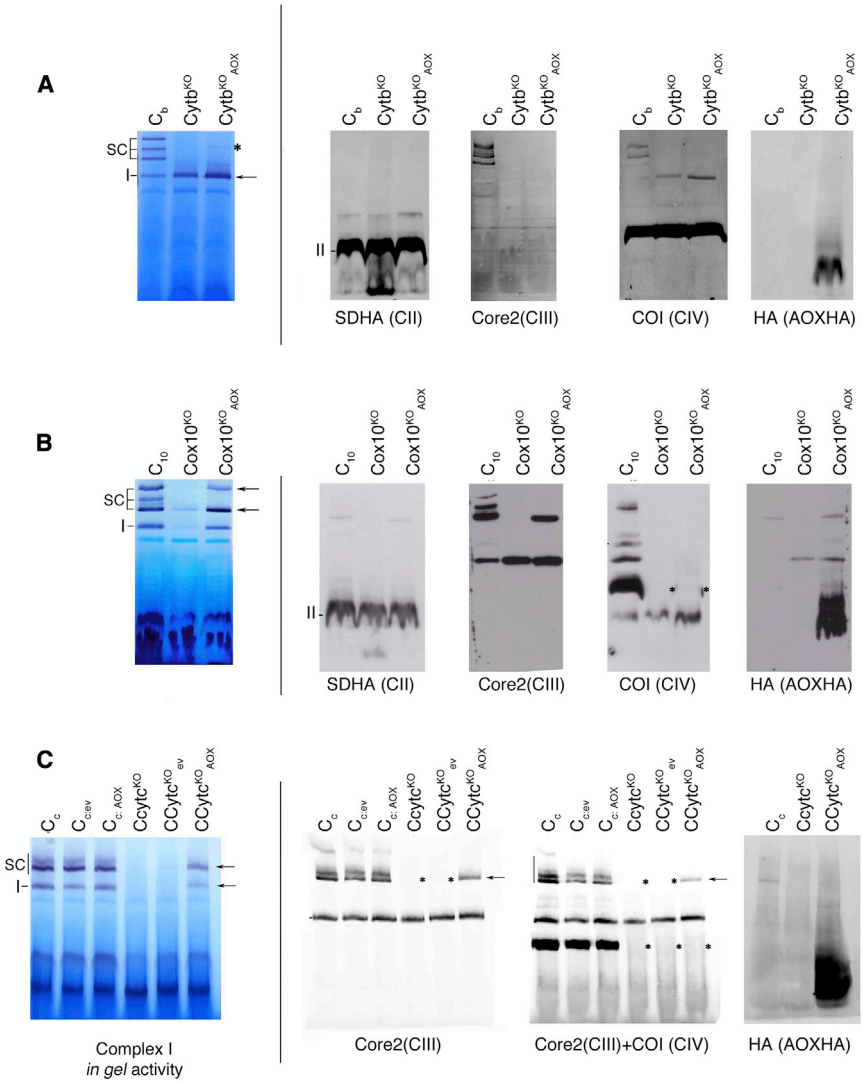

Figure 2. AOX Expression Stabilizes CI in the Absence of CIII, CIV, or cyt *c*

Restoration of assembled CI (arrows) was assessed by the detection of complexes and SCs in digitonin-solubilized mitochondria by in-gel CI activity assay after development of the reaction for 1 hr and by western blot with the indicated antibodies against AOX-HA and components of CII, CIII, and CIV.

(A) $Cytb^{KO}$ and $Cytb^{KO}$AOX cells.

(B) $Cox10^{KO}$ and $Cox10^{KO}$AOX cells.

(C) $Cytc^{KO}$ and $Cytc^{KO}$AOX cells. C_b, C_{10} and C_c, isogenic control cells. ev, empty vector.

Arrows in (A)–(C) indicate CI-containing bands, while asterisk indicates positions where the expected complexes or SCs are absent.

(AOX) from *Emericella nidulans* (Perales-Clemente et al., 2008). The expression of AOX restored a normal $COQH_2$:COQ ratio (Figure 1D) and respiration (Figures 1E, 1G, and 1I) without inducing major changes in the overall CoQ content (Table S1), consistent with its ability to restore respiration in cells lacking mtDNA (Perales-Clemente et al., 2008). Interestingly, AOX expression recovered not only succinate (CII)-driven respiration but also rotenone-sensitive glutamate/malate (CI)-driven respiration (Figures 1F, 1H, and 1J), indicating recovery of CI function. Consistent with the activity data, analysis of the assembly status of respiratory complexes by BNGE detected increased amounts of assembled CI in $Cytb^{KO}$AOX cells (Figure 1A). No CIII-containing bands were observed in $Cytb^{KO}$ or $Cytb^{KO}$AOX cells (Figure 2A), even after overexposure of blots, and the absence of CIII prevented formation of SCs (Figures 1A and 2A). AOX expression promoted the formation of a new band, containing CI without $CIII_2$ or CIV, which was not investigated further (Figures 1A and 2A). Immunodetection of CII and CIV showed no variation in these assembled complexes (Figure 2A).

Restoration of CI (in SC CI+CIII) was pronounced in $Cox10^{KO}$AOX cells (Figures 1B and 2B), with no effect on CIV levels (Figure 2B). Similar results were observed in $Cytc^{KO}$AOX cells, with restoration of CI but no recovery of CIV (Figures 1C and 2C), confirming that the molecular bases for the absence of CI and CIV in $Cytc^{KO}$ cells are different. AOX stabilizes CI without physically interacting with it (Figures 2 and S1).

To further analyze CI stabilization by AOX, we selectively labeled mtDNA-encoded oxidative phosphorylation (OXPHOS) subunits by a 2-hr pulse with [^{35}S] Met-Cys and tracked incorporation of labeled proteins into fully assembled complexes over a 12-hr chase period. 1D BNGE analysis of labeled digitonin-solubilized mitochondria revealed the typical band pattern corresponding to isolated CI and SCs in control cells (Figure S2). Mutant cells contained all respiratory complexes except CIII (in $Cytb^{KO}$ and $Cytb^{KO}$AOX cells) and CIV (in $Cox10^{KO}$, $Cox10^{KO}$AOX, $Cytc^{KO}$, and $Cytc^{KO}$AOX cells) (Figure S2). The specific labeling of mtDNA-encoded subunits was resolved by 2D BN-SDS-PAGE. $Cytb^{KO}$, $Cox10^{KO}$, and $Cytc^{KO}$ cells are able to assemble CI, but the instability of CI in these cells is revealed by the presence of labeled assembly intermediates or degradation products (Figure S2). Expression of AOX prevented accumulation of these abnormal assemblies, stabilizing CI either as a free complex or in SC CI+CIII in cell lines in which CIII is assembled (Figure S2).

Rotenone Stabilizes CI in the Presence of High $CoQH_2$

Restoring electron flux would normalize the NAD^+/NADH ratio, TCA cycle function, and CoQ redox status. To determine whether destabilization of CI requires interaction with CoQ in conditions where metabolic fluxes are not restored, we blocked this interaction by adding rotenone, which competes with ubiquinone for binding to CI (Murphy, 2009). Rotenone

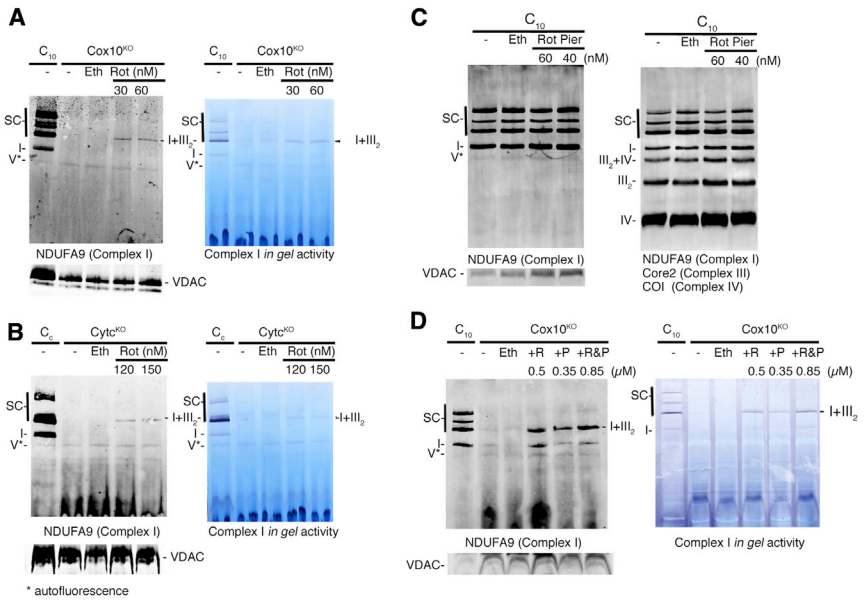

Figure 3. Rotenone Stabilizes CI in the Absence of CIV and cyt *c*

(A–D) Cells deficient for CIV ($Cox10^{KO}$ in A and D), cyt *c* ($Cytc^{KO}$ in B), or an isogenic control for $Cox10^{KO}$ (C_{10} in C) were treated for 48 hr at 21% O_2 with the indicated concentration of rotenone (Rot), piercidin A (Pier), or vehicle (ethanol; Eth). (A–D, left panels) Western blot after BNGE for CI (anti-NDUFA9) in digitonin-solubilized mitochondrial proteins; VDAC was detected as loading control. (A, B, and D, right panels) In-gel CI activity assay in BN gels incubated with NADH and nitroblue tetrazolium. (C, right) Parallel western blot after BNGE with the indicated antibodies.

concentrations >0.25 μM have mETC-unrelated toxic effects (Hofhaus and Attardi, 1995). To avoid confounding effects, we initially investigated the impact of low-nanomolar rotenone concentrations. At these concentrations, rotenone modestly stabilized CI in CIV^{KO} cells ($Cox10^{KO}$ and $Cytc^{KO}$) (Figures 3A and 3B) without influencing wild-type cells (Figure 3C). When rotenone concentration was increased to 500 nM, or when we used piercidin A, another antibiotic that competes with CoQ for interaction with CI, we found a stronger effect, confirming that blockade of CoQ-CI interaction without restoring electron flux stabilizes CI (Figure 3D).

Overexpression of SOD2 and Lowering of Oxygen Concentration Stabilizes CI

The CI-stabilizing effect of rotenone highlights the importance of the CoQ-CI interaction in CI degradation. When CoQ is reduced (high $CoQH_2$) because electrons cannot flow forward through CIII and CIV, they instead flow back to CI, a process known as RET. This backward flux can be induced by succinate, α-glycerophosphate, or β-oxidation and is critical in post-ischemia injury (Chouchani et al., 2014). When RET is induced, CI produces elevated amounts of superoxide (ROS), and this can be prevented by rotenone (Murphy, 2009). Overexpression of SOD2 in $Cox10^{KO}$ cells stabilized CI only weakly (Figures 4A and 4B), perhaps reflecting the inability of SOD2 to access and eliminate ROS generated in CI before they cause the oxidative damage that leads to degradation (Murphy, 2009).

As an alternative ROS-reducing strategy, we examined the effect of long-term cell culture at low oxygen concentration on the stability of CI in the mutants. Whereas acute hypoxia (minutes) induces mitochondrial ROS production, long-term hypoxia prevents ROS production (Hernansanz-Agustín et al., 2014). Culture at 1% O_2 for 48 hr stabilized CI in $Cox10^{KO}$ cells (Figure 4C). To confirm the influence of oxygen concentration, we exposed $Cox10^{KO}$ cells grown at 1% O_2 for 48 hr to different periods of reoxygenation at 21% O_2 (1, 4, and 7 hr). Upon reoxygenation, hypoxia-stabilized CI became unstable again (Figure 4D). Reoxygenation-induced CI degradation was prevented by rotenone (Figure 4E), and rotenone alone stabilized CI as efficiently as hypoxia in a time-dependent manner (Figure 4E).

Culturing $Cytc^{KO}$ cells in 1% O_2 induced a weaker, but still significant, CI stabilization (Figure 4F); in contrast, CIV was not restored. The third mutant, $Cytb^{KO}$, also clearly increased the steady-state level of CI upon 3-day culture at 1% O_2 (Figure 4G). In wild-type cells (Cb), 1% O_2 slightly but conspicuously affected the distribution of CI in SCs, with reductions in the levels of free CI and the respirasome (CI+CIII+CIV) (Figure 4G).

The observed effect was not mediated by decreased $CoQH_2$ accumulation (Figure S3A). Hypoxia also promotes a general transcriptional response by stabilizing hypoxia-induced transcription factors (Koh and Powis, 2012). To determine whether the HIF1α-dependent transcriptional program influences hypoxia-induced CI stabilization and reoxygenation-induced degradation, we stabilized HIF1α in normoxia by treating CIV^{KO} cells with dimethyloxallyl glycine (DMOG), an inhibitor of PHF and FIH-1 that upregulates HIF-1α. After 72-hr exposure to DMOG or hypoxia, the HIF1α-dependent transcription program was robustly activated in control and $Cox10^{KO}$ cells, as indicated by increased mRNA expression of the HIF1α targets Pdk1 and Phd3 (Figure S3B). However, activation of the HIF1α program by DMOG in normoxia did not stabilize CI (Figure S3C).

Oxidation of CI Proteins Precedes CI Degradation

In contrast with assembled CI, total CI proteins (assembled or not) stabilized by hypoxia increased initially upon reoxygenation and then decreased over 12 hr to the levels seen in hypoxia (Figure S4A). To define the time-course behavior of individual CI proteins, we conducted a quantitative proteomics analysis by ^{18}O stable isotope labeling and mass spectrometry. Hierarchical clustering analysis of protein amounts, validated by western blot determinations, revealed distinct stability behaviors that cluster the proteins into at least four groups (Figures 5A and 5B). The least stable group contains subunits of the dehydrogenase and hydrogenase modules NDUFV1, NDUFV2, NDUFS2, and NDUFS3 and others in the peripheral arm of CI (Figure 5A).

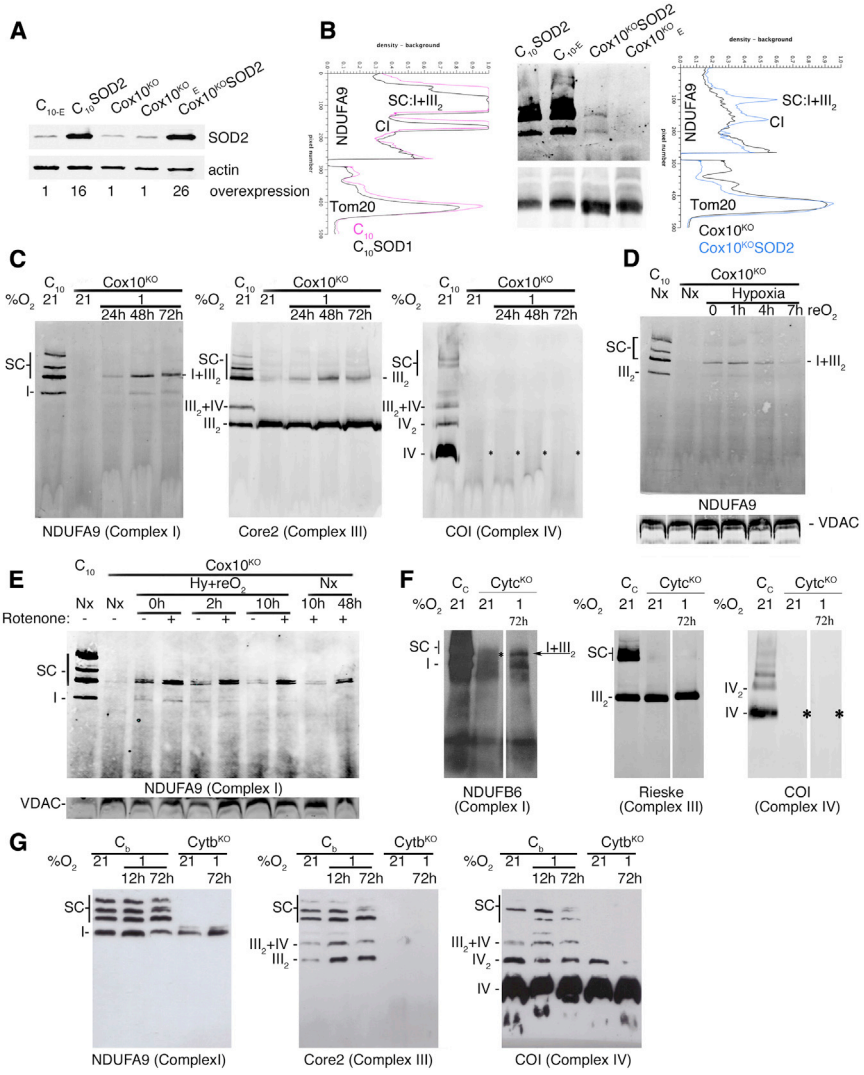

Figure 4. ROS Generation Blockade Stabilizes CI

(A) Western blot after SDS-PAGE showing mitochondrial overexpression of SOD2 in C_{10} or $Cox10^{KO}$ cells. E subindex, empty vector.

(B) Center: western blot after BNGE for CI (anti-NDUFA9) or Tom20 (loading control) in digitonin-solubilized mitochondrial proteins from C_{10} or $Cox10^{KO}$ cells overexpressing SOD2. Left: densitometry traces of lines 1 and 2 of the gel. Right: densitometry traces of lines 3 and 4 of the gel.

(C) BNGE and western blot of digitonin-solubilized mitochondrial proteins isolated from wild-type cells (C_{10}) or cells lacking CIV ($Cox10^{KO}$) cultured at 21% O_2 or 1% O_2 for the indicated times. Blots were probed with the antibodies indicated below the blots to detect CI (left), CIII (center), or CIV (right).

(D and E) BNGE of digitonin-solubilized mitochondrial proteins from control cells (C_{10}) or cells lacking CIV ($Cox10^{KO}$) cultured for 72 hr (D) or 48 hr (E) at 1% O_2 to stabilize CI and then transferred to 21% O_2 to track the fate of CI over the indicated periods in the absence or presence of rotenone. (E) Lines 9 and 10, time course of rotenone-induced CI stabilization in normoxia (Nx).

(F) Analysis as in (C) of mitochondrial proteins isolated from control cells (Cc) or cells lacking cyt *c* ($Cytc^{KO}$) cultured at 21% or 1% O_2.

(G) Analysis as in (C) of mitochondrial proteins isolated from control cells (Cb) or cells lacking CIII (cytochrome b deficient; $Cytb^{KO}$) cultured at 21% or 1% O_2.

$CIII_2$, CIII dimer; $I+III_2$, SC containing CI and CIII; III_2+IV, SC containing CIII and CIV. Asterisks in (C and F) highlight CIV depletion.

A second cluster follows a slightly delayed degradation pattern and includes NDUFS1 and NDUFS7 from the hydrogenase module, as well as the accessory peripheral arm subunits NDUFA2 and NDUFA12 (Figures 5A and 5B). Clusters 3 and 4 contain stable proteins (among them, NDUFA9) that are subunits of the CI membrane arm (Figures 5A and 5B). Notably, protein components of the other OXPHOS complexes did not show a pattern of changes consistent with their degradation (Figure S4B). These observations suggest that reoxygenation produces protein degradation locally within CI, particularly in the dehydrogenase and hydrogenase modules. In fact, the more stable proteins (cluster 4), such as NDUFA9, can be detected in subcomplexes in cells lacking CIV (Figure 5C).

To determine the relationship between protein degradation and oxidative damage, we performed a high-throughput, data-independent, quantitative redox proteomics analysis with GELSILOX (Martínez-Acedo et al., 2012) of mitochondrial proteins of $Cox10^{KO}$ cells grown under hypoxia to stabilize CI and after different periods of reoxygenation. The screen detected 1,068 cysteines from 784 proteins out of the 1,098 proteins described in MitoCarta (Pagliarini et al., 2008). After 72 hr at 1% O_2, the overall proportion of cysteine-containing peptides identified in the oxidized state in mitochondrial proteins was quite low, at around 16%. This quickly increased when the cultures were moved to 21% O_2, peaking after 4 hr at 22%, and dropping again with prolonged normoxia (Figure S4C). This effect was particularly pronounced for the protein components of CI, whose proportion of oxidized cysteines increased from 32% at 1% O_2 to 50% after 4 hr at 21% O_2 (Figure S4C). In contrast, CII did not show such a pronounced increase, following instead the overall pattern of total mitochondrial cysteines (Figure S4C). Interestingly, a peak in oxidized cysteines at 4-hr reoxygenation was also observed for components of CIII (Figure S4C), the complex that partially superassembles with CI, despite the absence of signs of degradation of CIII subunits (Figure S4B).

Cysteines monitored in NDUFS5, NDUFA8, and NDUFB7, which face the mitochondrial intermembrane space, were only detected in the oxidized form (Figure 5D), consistent with their likely participation in stable intramolecular disulfide bonds (Szklarczyk et al., 2011). NDUFV1 and NDUFS1 are subunits of the NADH dehydrogenase module, and NDUFS2 is a subunit

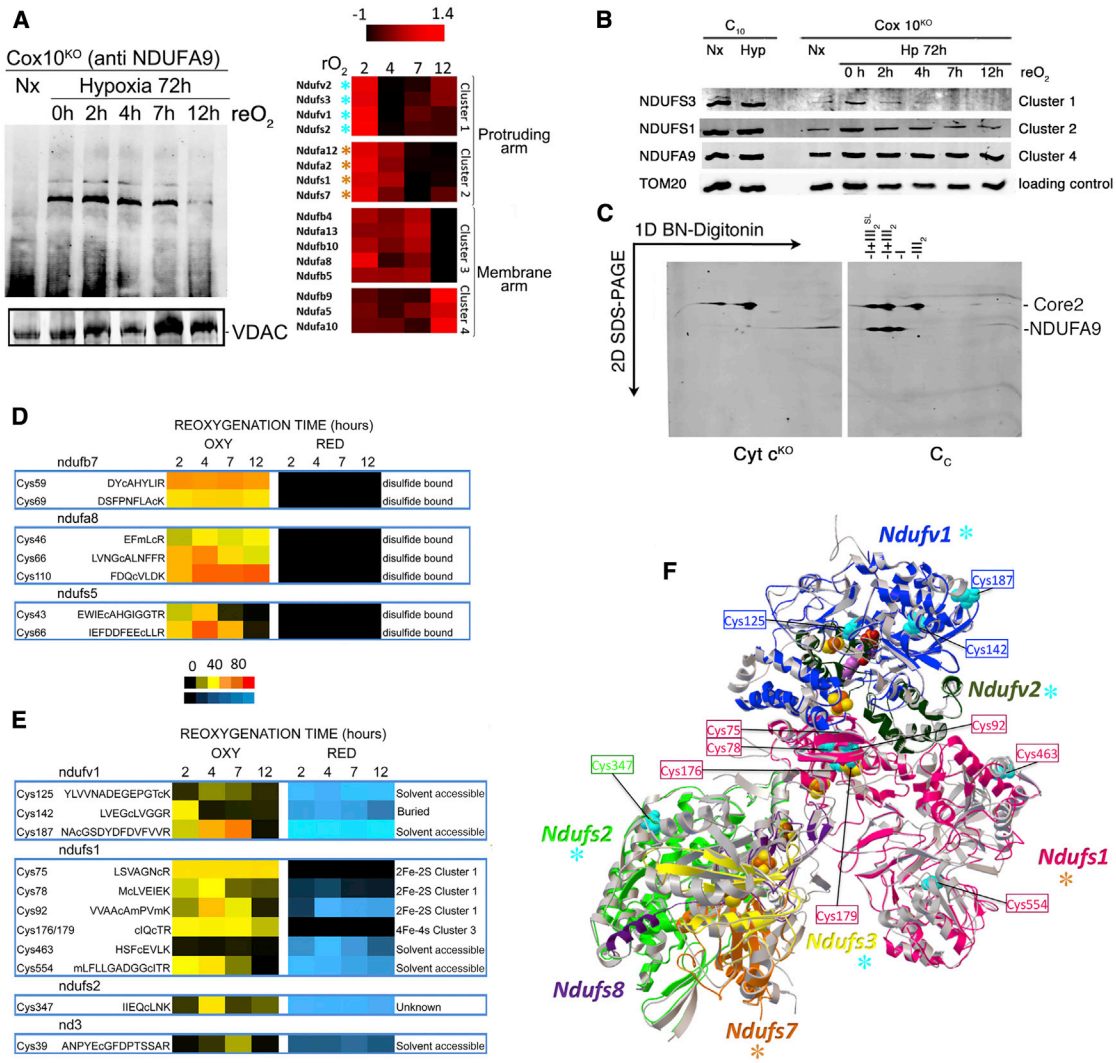

Figure 5. Mass Spectrometry Analysis of Oxidative Alterations in CI Proteins from CIV-Deficient Cells

(A) Left: immunodetection of CI (anti-NDUFA9) after BNGE of digitonin-solubilized mitochondria grown in normoxia (Nx), hypoxia (Hypoxia 72 h) and after the indicated times of posthypoxia reoxygenation (reO_2). VDAC was immunodetected as a loading control on the BN gel. Right: Heatmap showing the timing of degradation of individual CI proteins after posthypoxia reoxygenation. Color intensity represents the change in protein concentration in relation to the hypoxia condition, in log_2-ratio units, determined by quantitative proteomics ($^{16}O/^{18}O$ isotope labeling). Four groups of proteins, classified according to stability, were obtained by hierarchical clustering analysis (Genesis v 1.7.6, Institute of Molecular Biotechnology, Graz University of Technology). The clustering groups proteins that are in physical contact in the CI structure; the less stable proteins are those in the protruding arm of CI (clusters 1 and 2), and the more stable are those in the membrane arm (clusters 3 and 4).

(B) Western blot validation of the differential stability detected by proteomics upon hypoxia (Hx) and reoxygenation.

(C) Immunodetection of Ndufa9 after BNGE followed by second-dimension SDS-PAGE in cells lacking cyt *c* ($Cytc^{KO}$) and isogenic controls (C_c), both grown in normoxia (Nx). Core 2 (CIII protein) and NDUFA9 (CI protein).

(D and E) Semiquantitative heatmap analysis of the relative levels of oxidized (OXY) and reduced (RED) cysteine-containing peptides from the indicated mitochondrial proteins detected by data-independent DiS-MS, as assessed by SpScore (used by SEQUEST to rank peptide candidates), according to the indicated color scales. Peptides were obtained from mitochondria of $Cox10^{KO}$ cells grown in hypoxia (1% O_2, 72 hr) and after reoxygenation (21% O_2) for the indicated times. The proposed roles of cysteine oxidation status are indicated in (D) (peptides from CI subunits facing the intermembrane space: NDUFB7, NDUFA8, and NDUFS5) and (E) (peptides from matrix-protruding subunits: NDUFV1, NDUFS1, NDUFS2, and ND3).

(F) Localization of subunits and detected cysteine sites (cyan) in the modeled CI structure; the FMN group is shown in purple, and the Fe-S centers in yellow/red. The colored asterisks indicate stability of the proteins as shown in (A).

of the hydrogenase module (Figure 5F). All three locate at the hydrophilic protrusion of CI into the mitochondrial matrix. The detailed structure of mammalian CI is still not fully resolved (for an updated model, see Hirst, 2013 and Vinothkumar et al., 2014), but that of *T. Thermophilus*, which contains NDUFV1, NDUFS1, and NDUFS2 orthologs (Nqo1, Nqo3, and Nqo4), has

been resolved (Baradaran et al., 2013; Efremov et al., 2010). None of the three cysteines detected in NDUFV1 are conserved in Nqo1 (Table S2), but five of the seven cysteine residues detected in NDUFS1 are conserved in Nqo3 and coordinate iron-sulfur cluster 1 (Cys^{75}, Cys^{78}, and Cys^{92}) and cluster 3 (Cys^{176} and Cys^{179}). The only cysteine site monitored in NDUFS2 (Cys^{347}) is not conserved in Nqo4. In these proteins, the profile of detected oxidized forms changed after reoxygenation, but the cysteine sites in the same or different proteins showed defined response patterns (Figure 5E). The three cysteine sites in NDUFV1 were found in both the oxidized and reduced states (see Figures S4D and S4E for a representative example), but in all cases, the oxidized form was more sensitive to reoxygenation, rising to a maximum at 2 hr for Cys^{142}, 4 hr for Cys^{125}, and 7 hr for Cys^{187}, followed in all cases by rapid disappearance, suggesting that the oxidized forms are unstable upon reoxygenation (Figure 5E). Although the role of these cysteine sites is unknown, computer simulations suggest that Cys^{125} and Cys^{187} are solvent accessible, whereas the more sensitive Cys^{142} is buried in the protein (Figure 5F). A similar pattern was detected for a cysteine site monitored in NDUFS2, whose oxidized form reached a maximum at 4 hr post-reoxygenation and then dropped away. In NDUFS1, Cys^{75}, Cys^{176}, and Cys^{179} were only found in the oxidized state, in agreement with their role in the formation of iron-sulfur clusters, where they are not expected to be directly accessible to alkylation before treatment with the reducing agent (Figure 5E). In contrast, Cys^{78} and, more clearly, Cys^{92}, part of iron-sulfur cluster 1, showed marked sensitivity to reoxygenation, with the reduced forms progressively replacing the oxidized forms, suggesting progressive damage to the iron-sulfur cluster. NDUFS1 residues Cys^{463} and Cys^{554} were mainly detected in the reduced form, consistent with their likely exposure to solvent (Figure 5F). Cys^{554} showed a transient increase in oxidation that peaked 4 hr after reoxygenation. Interestingly, Cys^{463} and Cys^{554} are reported to be sensitive to oxidation upon glutathione depletion in brain mitochondria (Danielson et al., 2011) (Table S2).

Cys^{347} in NDUFS2 and Cys^{39} in ND3 were mainly detected in the reduced form. Interestingly, these sites also showed transient increases in oxidation at 4 and 7 hr, respectively. While the role of Cys^{347} is unknown, Cys^{39} is implicated in the transition between the activated and deactivated forms of CI in response to myocardial ischemia/reperfusion injury (Galkin et al., 2008). In agreement with predictions by Galkin et al., we found this cysteine to be very exposed after hypoxia (Galkin et al., 2009); the peak in its oxidation at 7 hr reoxygenation may reflect the instability of CI upon recovery of the functional oxidized form, since this coincides with its preferential elimination.

Taken together, these data indicate that reoxygenation produces the transient oxidation of critical cysteine sites, among them, those located in iron-sulfur clusters in the hydrogenase and NADH dehydrogenase CI modules. The destabilization of iron-sulfur clusters and of other critical cysteine sites probably induces degradation of subunits within these modules, in turn, triggering the disassembly of CI, thus providing a potential molecular explanation that links specific cysteine oxidation to the differential stability and degradation of CI proteins during reoxygenation.

RET Regulates the Physiological CI/CII Balance

Inhibition of the activity of CIII and CIV in wild-type cells did not induce complete CI degradation, but significantly reduced the amount of CI and specifically affected its superassembly status (Figures 6A–6D). This is consistent with our earlier observation that pharmacological inhibition of CIII activity does not fully mimic the effect of physical ablation of CIII on CI stability (Acín-Pérez et al., 2004). The decrease in CI induced by pharmacological inhibition of CIII or CIV was prevented by rotenone (Figures 6C and 6D), linking the CI stabilization effect of rotenone in mutant and wild-type cells.

Next, we reproduced in cultured cells our in vivo observation that the mETC adapts to fuels that generate different proportions of NADH and $FADH_2$ by increasing or reducing the amount of CI (Lapuente-Brun et al., 2013). Wild-type cells were fed one of three carbon sources: galactose, glucose, or FAs (AlbuMAX). The switch from glucose to galactose maintains the same feed to the mETC through pyruvate and thus should not alter the NADH:$FADH_2$ ratio; this switch did not induce major changes in CI amount or superassembly status (Figure 6A, right panel; Figure S5A). In contrast, switching from glucose to FAs should decrease the NADH:$FADH_2$ ratio, and in this case, it induced a reduction of CI content, reproducing the effect of inhibiting CIII or CIV, with a more marked effect on free CI and the slow-migrating CI+CIII SC than on fast-migrating CI+CIII (Figure 6A, right panel; Figure S5A). Note that the cells used in Figure 6A were derived from C57BL/6J mice and lack SCAFI; therefore, they are unable to assemble CIV into SCs (Lapuente-Brun et al., 2013). Switching to FAs in SCAFI-positive cells triggered a similar reduction in total CI, which was more evident in slow-migrating CI+CIII and CI+CIII+CIV (Figure 6B, right panel; Figure S5B). To evaluate whether there is a correlation between substrates that yield different NADH:$FADH_2$ electron ratios and adjustments to the proportion of CI, we tested the consequences of feeding cells with ketone bodies instead of glucose (Figures 6E and 6F). An equimolar mix of beta-hydroxibutirate (K-HB) and acetoacetate would theoretically yield a NADH:$FADH_2$ electron ratio of 3.5, well below the ratio of 5 that was obtained with glucose or galactose. In both SCAFI-positive and SCAFI-negative cells, ketone bodies induced a reduction in CI similar to that promoted by FA (Figure 6E and 6F).

As expected, inhibition of electron flux downstream of CoQ by pharmacological inhibition of CIII or CIV significantly increased CoQ reduction, and this effect was blocked by rotenone (Figure 6G). The change in carbon source that induced reduction in CI correlated with an FA-induced elevation in $CoQH_2$ (Figure 6G) and with elevated ROS production (Figure 6H). Moreover, FA-induced ROS elevation was prevented by rotenone, which nonetheless induced ROS in galactose-fed cells (Figure 6H). Thus, the switch from glucose to FA increases $CoQH_2$, promoting RET and leading to CI degradation.

To confirm a direct link between RET and CI-degradation-mediated mETC remodeling in wild-type cells, we activated CII by enhancing its phosphorylation by the H_2O_2-triggered tyrosine kinase Fgr (Acín-Pérez et al., 2014; Nath et al., 2015). This was achieved by adding xanthine and xanthine oxidase to the culture medium to generate H_2O_2, thereby enhancing delivery of $FADH_2$ electrons to CoQ (Acín-Pérez et al., 2014). H_2O_2 derived from

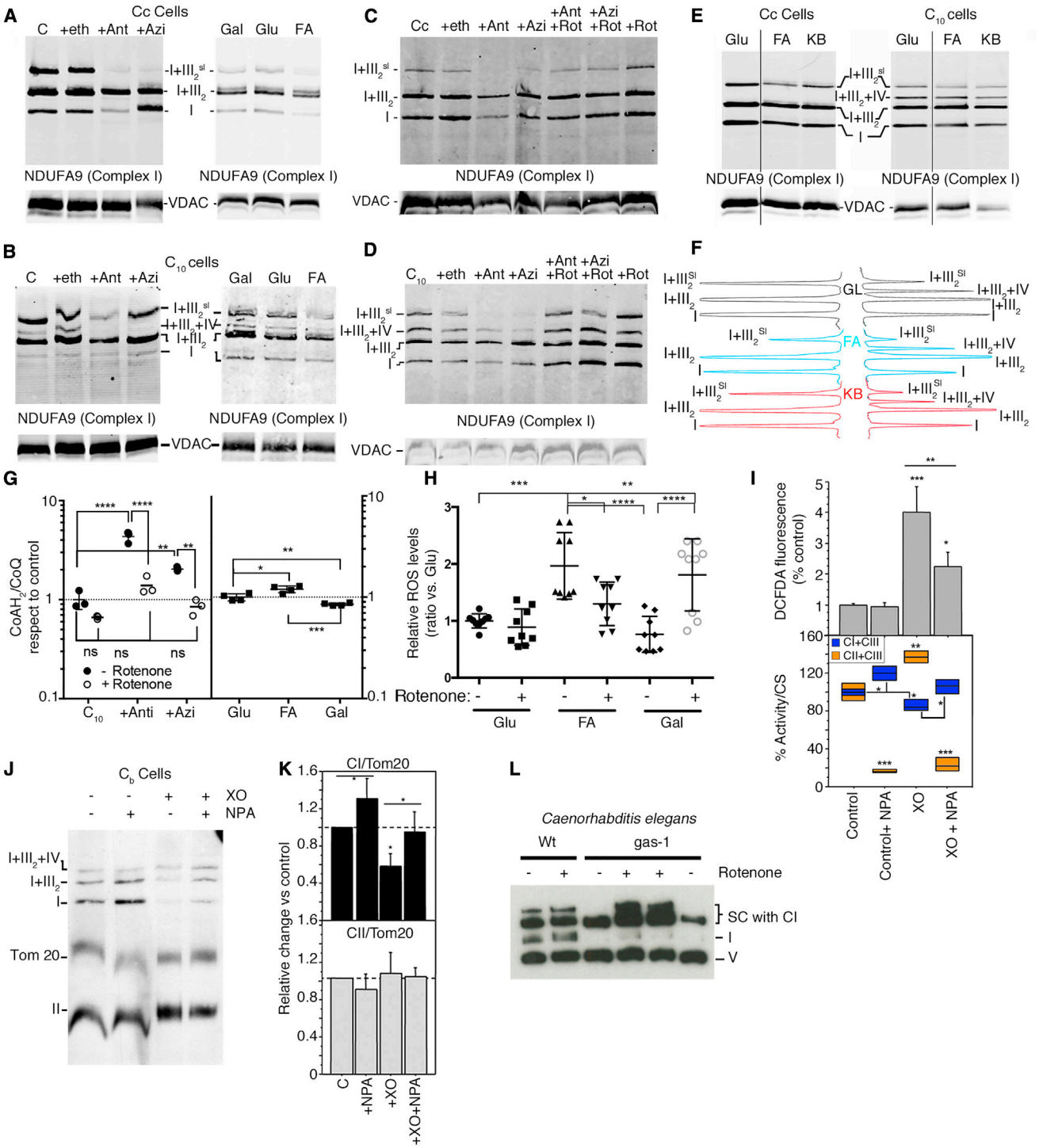

Figure 6. Activation of Electron Flux through the FAD Pathway, by FAs or Activation of CII, Downregulates CI Content

(A–D) In (A) and (B), left, and (C) and (D), control cells isogenic for the Cyt c^{KO} line (Cc) or the $Cox10^{KO}$ line (C_{10}) reorganize CI superassembly and amount upon pharmacological inhibition (48 hr) of CIII with antymycin A (+Ant), CIV with azide (+Azi), or CI with rotenone (+Rot); eth, ethanol (vehicle). (A and B, right) CI remodeling 24 hr after changing the carbon source from glucose (Glu) to galactose (Gal) or FAs in Cc or C_{10} cells.

(E) CI remodeling 24 hr after changing the carbon source from Glu to FA or ketone bodies (KB) in Cc or C_{10} cells.

(F) Densitometric traces of the electrophoretic lines shown in (E).

(G) $CoQH_2$/CoQ fold change rate after inhibition of CIII or CIV with the indicated drug in the presence or absence of rotenone or 24 hr before fuel shift. Data are mean ± SD; n = 3–4.

(legend continued on next page)

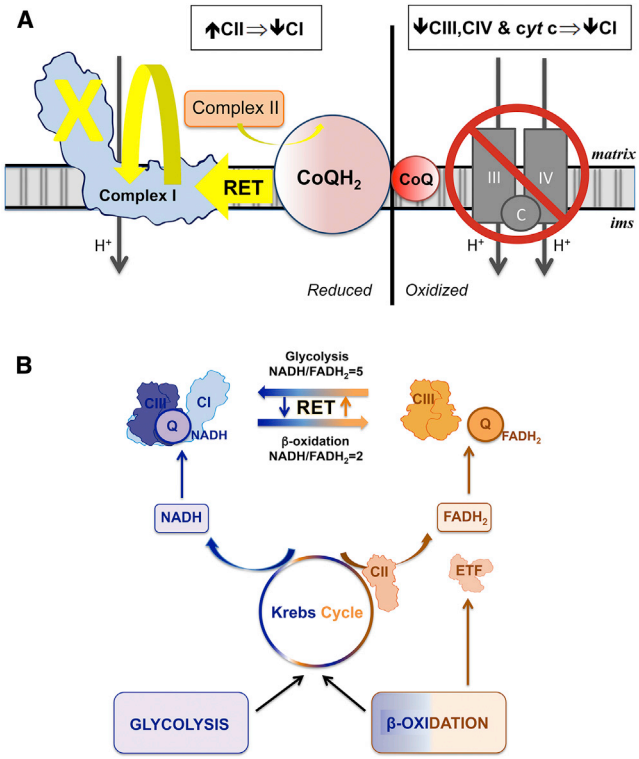

Figure 7. Proposed Physiological Role of RET

(A) Model of the relationship between RET from CoQ to CI, superoxide production at CI, and concomitant oxidative tagging of CI for degradation.

(B) Model of the physiological role of RET. Different fuel sources generate a characteristic ratio of NADH- and $FADH_2$-derived electrons. The mETC reconfigures to optimize oxidation capacity. When delivery of $FADH_2$ electrons surpasses a threshold, RET is induced and CI degraded, liberating CIII to oxidize CoQ_{FAD}, thereby reducing RET. ETF: electron transfer flavoprotein.

xanthine oxidation was readily detected (Figure 6I). Inhibition of CII with nitropropionic acid in H_2O_2-treated cells significantly reduced ROS, indicating that the addition of external H_2O_2 triggers a second wave of H_2O_2 from an internal source that requires CII activity (Figure 6I). Inhibition of CII in the absence of H_2O_2 increased CI+CIII activity and the relative amount of assembled CI, whereas activation of CII with H_2O_2 had the opposite effect (Figures 6I–6K). H_2O_2-induced CI loss was prevented by CII inhibition with nitropropionic acid and in cells lacking Fgr kinase (SF5C) or with a mutated target tyrosine in the 70Kd CII subunit (SF5D). The FgrKO and CII-phosphorylation-deficient cells both had low CII activity that was insensitive to activation by externally derived H_2O_2 (Figures S5C and S5D). CI activity in these cells was not inhibited by xanthine and xanthine oxidase, showing that this inhibition requires CII activation (Figures S5C and S5D). These experiments establish a causal link between RET and the loss of CI in wild-type cells upon activation of delivery of $FADH_2$ electrons (Figure 6). To evaluate whether this mechanism operates in vivo, we examined the natural *Caenorhabditis elegans* mutant gas-1, whose abnormally high CII expression destabilizes CI (Pujol et al., 2013). The gas-1 mutants were highly sensitive to low-dose rotenone (Table S3), and 10 hr on this low dose significantly stabilized CI (Figure 6L).

DISCUSSION

Our results allow us to propose a molecular mechanism through which mitochondria reconfigure the mETC to adjust to the ratio of electron flux from NADH and $FADH_2$ (Figure 7). The function of CoQ redox status as a metabolic sensor enabling cells to adjust the amount of NADH dehydrogenase (CI) explains the structural dependency of CI on CIII and CIV and the variability of biochemical defects in patients with OXPHOS deficiencies in a single mETC component (Bruno et al., 2003; Lamantea et al., 2002). We also reveal a relationship between CII and CI, whereby CI is destabilized not only by CIII or CIV deficiency but also by activation of CII. In all cases, $CoQH_2$ accumulation triggers RET (Figure 7A), causing localized damage to CI components and disassembly of the complex until it reaches the appropriate level. Thus, less CIII is dedicated to CI+CIII SCs, potentiating oxidization of $CoQH_2$ generated by FAD-dependent enzymes. This mechanism links CoQ redox status to the recently described role of the SC organization of mitochondrial respiratory complexes (Lapuente-Brun et al., 2013) and adds a second route for SC regulation in addition to the remodeling of cristae shape (Cogliati et al., 2013).

The loss of CI upon excess expression of CII in *C. elegans* (Pujol et al., 2013) and its reversal by CII downregulation (Pujol et al., 2013) or rotenone treatment (as discussed in this article) extend the relevance of CoQ redox status in ETC remodeling to distant metazoans. Moreover, AOX, which restores CI by oxidizing $CoQH_2$, is proposed to contribute to the assembly or stability of fungal CI (in *Podospora anserina* mutants, in which respiration relies exclusively on AOX due to the lack of CIII and CIV [Krause et al., 2004; Maas et al., 2009], and in other microorganisms, including *Yarrowia lipolytica* [Guerrero-Castillo et al., 2009] and

(H) Flow cytometry analysis of ROS production 24 hr after fuel shift in the presence or absence of rotenone. Data are mean ± SD; n = 9.

(I) Top: flow cytometry analysis of ROS production in Cb cells treated with xanthine oxidase + xanthine (XO) to generate H_2O_2; nitropropionic acid (NPA) was added as a CII inhibitor. Bottom: effect of H_2O_2 on CII and CI activities in control cells (Cb) upon CII inhibition (+NPA), CII stimulation (+XO), or simultaneous treatment with NPA and XO. Data are normalized to citrate synthase activity (CS). Data are represented as a boxplot; n ≥ 4.

(J) BNGE of digitonin-solubilized mitochondrial proteins from control cells (C_b) cultured in the presence of the indicated drugs, illustrating adjustment in the relative amounts of CI and CII. The blot shows immunodetection of CI (anti-NDUFA9), CII (anti-FpSDH), and Tom20 as a loading control; positions of complexes and superassemblies are indicated on the left.

(K) Quantification of changes in CI and CII content shown in (J).

(L) BNGE of mitochondrial preparations from two *C. elegans* strains: control (Wt) and the natural CII-overexpressing mutant gas-1. Superassembly of CI is impaired in gas-1 worms, but the normal pattern of CI SCs is restored upon in vivo RET blockade with rotenone.

Statistical differences were assessed by ANOVA Tukey's multiple comparisons test. *p < 0.05; **p < 0.01; ***p < 0.001; ****p < 0.0001.

Neurospora crassa [Duarte and Videira, 2009]); however, no explanation has been offered of how AOX might achieve this. AOX-mediated prevention of increase in $CoQH_2$, as detected here in mammalian mitochondria, provides a convincing explanation, suggesting that this mechanism operates in fungi and is, therefore, very ancient.

Our proteomics analysis reveals oxidative alterations in a defined CI region: the NADH dehydrogenase and hydrogenase modules. Subunits of these modules are degraded faster than most other CI subunits, with NDUFV1 and NDUFS1 appearing to be the most sensitive components. The cysteines monitored in these two proteins participate in the linking of iron-sulfur clusters or are solvent accessible; therefore, their oxidation may cause loss of the cluster. Interestingly, these CI subunits are the most sensitive to the knockdown of the iron-sulfur cluster assembly factor Ind1, whereas proteins of the CI membrane arm are less affected (Sheftel et al., 2009). In agreement with this view, independent reports showed that the subunits from NADH module can be replaced in pre-existing CI and are more rapidly turned over than other CI subunits (Dieteren et al., 2012; Lazarou et al., 2007).

CI is believed to be a major site of ROS production in the mETC, either from FAD- or NAD-driven electron flux (Murphy, 2009). NADH feeds electrons to CI via forward electron transfer (FET), and this can lead to ROS production when downstream electron flux is inhibited, for example, by rotenone (Murphy, 2009; Ten and Starkov, 2012). However, under specific conditions, these electrons can flux back to CI through $CoQH_2$ via RET. It is notable that RET, but not FET, promotes CI degradation. The reason for this is unclear and just may be due to the fact that RET induces much more ROS than FET, or it may suggest that the manner of electron flux within CI may be relevant to the proposed regulatory role of CoQ redox status.

RET has been demonstrated in isolated mitochondria (Murphy, 2009; Ten and Starkov, 2012), and its physiological role in vivo has been highlighted recently by the description of its major contribution to cardiac ischemia/reperfusion injury associated with myocardial infarction (Chouchani et al., 2014). Here, we extend ideas of RET function beyond pathology to a fundamental physiological role as a mechanism that fine-tunes mitochondrial OXPHOS to the available carbon source.

EXPERIMENTAL PROCEDURES

Cell Lines and Media

All cell lines were grown in DMEM (D5796 Sigma-Aldrich) supplemented with 5% FBS (fetal bovine serum, GIBCO-BRL) and 1 mM sodium pyruvate (Lonza) in a 5% CO_2, 95% air atmosphere at 37°C. Cell lines lacking a mitochondrial complex were supplemented with 50 μg/ml uridine. The different cell lines used in this study were generated and described previously: *mt-CYTb* mutant lacking CIII, called $Cytb^{KO}$ here and A22 in a previous report (Acín-Pérez et al., 2004); the $COX10^{KO}$ cell line, lacking CIV (Diaz et al., 2006); and $Cytc^{KO}$ cells (Vempati et al., 2009). For hypoxic exposure, cells were placed in a modular incubator chamber (Ruskinn) that was flushed with 1% O_2/5% CO_2/balance N_2. For drug treatment, medium containing the indicated concentration of rotenone, antymycin A (125 nM), or azide (1 mM) was changed daily, and cells were cultured for 48 hr. When indicated, cells were cultured for 24 hr in sugar-free DMEM (Sigma-Aldrich D5030) supplemented with 5% dialyzed FBS, 1 mM sodium pyruvate (Lonza), and 2 mM L-glutamine (Lonza) and further supplemented, as required, with 5 mM glucose, 5 mM galactose, 1 mg/ml lipid-rich bovine serum AlbuMAX (GIBCO) plus 0.5 mM L-carnitine hydrochloride (Sigma) or a mix of lithium acetoacetate (5 mM) plus DL-beta-hydroxybutyric acid sodium salt (5 mM).

Gene Constructs

The mouse codon-usage-optimized version of the *Aox* gene from *Emericella nidulans* was utilized as previously described (Perales-Clemente et al., 2008).

CoQ Determination

CoQ content and the ratio of the oxidized and reduced forms were measured as described previously (Brea-Calvo et al., 2006; Lagendijk et al., 1996).

Quantitative Real-Time PCR

Total RNA was extracted from 1 million of cells with TRIzol, followed by purification with a commercial kit (QIAGEN). Quantitative real-time PCR was performed with primers for Pdh3 (forward, 5′-TGGACAACCCCAATGGTGAT-3′, reverse, 5′-GCAGGACCCCTCCATGTAACT-3′) and Pdk1 (forward, 5′-AGCA GTTCCTGGACTTCG-3′, reverse 5′-CTCCTGAAGGCTTTGGATATACC-3′).

Mitochondrial Proteomics by Data-Independent Scanning Mass Spectrometry

Mitochondrial cysteine-thiol redox status was studied using the GELSILOX method (Martínez-Acedo et al., 2012). 1% false discovery rate (FDR) was used as a criterion for peptide identification; this parameter was estimated using a separate inverted database (Navarro and Vázquez, 2009). After protein digestion with trypsin, the resulting peptide mixtures were analyzed by data-independent scanning (DiS) onto a Q-Exactive mass spectrometer (Thermo Fisher Scientific). Each sample was analyzed in two chromatographic runs covering different mass ranges (from 400 to 750 Da and from 750 to 1,100 Da, respectively). The DiS cycle consisted of 175 sequential HCD MS/MS (higher energy C-trap dissociation/tandem mass spectrometry) fragmentation events with 2-Da windows. Semiquantitative monitorization of identified peptides was performed in the MS/MS spectra using Sequest's SpScore. 1% FDR was used as a criterion for peptide identification; this parameter was estimated using a separate inverted database (Navarro and Vázquez, 2009). Detailed description of the proteomic analysis can be found in the Supplemental Information.

Quantitative Analysis of Mitochondrial Proteins

After in-gel trypsin digestion, all the reoxygenation samples were equally mixed with a control sample (hypoxia) labeled with ^{18}O. Peptide quantification from FullScan spectra and labeling efficiency calculation were performed as described previously (López-Ferrer et al., 2006; Ramos-Fernández et al., 2007)

Lentiviral Vector Production and Transduction of Cell Lines

Lentiviral vectors were generated as described previously (Naldini et al., 1996). Cells at 80% confluence were transduced with lentiviral particles carrying the *Aox* or *SOD2* gene. Cells expressing the protein of interest were isolated by puromycin selection.

BN Electrophoresis and In-Gel Activity Assay

Mitochondria were isolated and analyzed by BNGE, according to Wittig et al. (2006), with some modifications (Acín-Pérez et al., 2008). SDS-PAGE was conducted with strips excised from the first-dimension BNGE (Wittig et al., 2006).

Western Blotting

After electrophoresis (SDS-PAGE, BNGE, or BN-SDS-PAGE), gels were electroblotted onto Hybond-P polyvinylidene fluoride (PVDF) membranes (GE Healthcare) and sequentially probed with specific antibodies against CI components (anti-NDUFA9 from MitoSciences; anti-NDUFB6 from Molecular Probes; and anti-NDUFA8, anti-NDUFB7, and anti-NDUFS5 from Protein Tech), CII (anti-70 kDa subunit from Molecular Probes), CIII (anti-Core2 from MitoSciences), CIV (anti-COI from MitoSciences), VDAC1 (MitoSciences), Tom 20 (Santa Cruz Biotechnology), AOX-HA (anti-hemagglutinin [anti-HA] from Roche), and SOD2 (Abcam). Secondary antibodies were peroxidase conjugated (Invitrogen) when the signal was generated using ECL Plus (GE

Healthcare) or conjugated to LI-COR IRDye 800CW or IRDye 680LT when the signal was acquired with the ODYSSEY Infrared Imaging System (LI-COR). The relative amount of each band was estimated with GelEval software from the scanned membranes or with the ODYSSEY Infrared Imaging System (LI-COR). The traces obtained by vertical scan represent the density along the line.

Pulse Labeling of mtDNA-Encoded Subunits

Cysteine residues in mtDNA-encoded proteins were labeled in intact cells with [^{35}S]-methionine during a 2-hr pulse followed by a 12-hr chase, using the EXPRE^{35}S^{35}S Protein Labeling Mix (PerkinElmer Life Sciences), as described elsewhere (Chomyn, 1996; Fernández-Silva et al., 2007).

Oxygen Consumption

Oxygen consumption was measured with an XF96 Extracellular Flux Analyzer (SeaHorse Bioscience), as specified by the provider. Data were normalized to DNA content with the CyQuant NF Cell Proliferation Assay Kit (Molecular Probes). Oxygen consumption in digitonin-permeabilized cells was measured with an Oxytherm Clark-type electrode (Hansatech), as previously described (Bayona-Bafaluy et al., 2003).

Immunofluorescence

Cells were incubated for 20 min under culture conditions with 100 nM of the mitochondrial dye MitoTracker Red (Molecular Probes). Cells were fixed with 4% paraformaldehyde and permeabilized with cold methanol. After blocking with 2% BSA, cells were incubated with anti-HA antibody (Roche) and Alexa Fluor 488 secondary antibody (Molecular Probes).

Immunoprecipitation

CI was immunocaptured from digitonin-solubilized mitochondria with the MitoSciences CI Immunocapture Kit.

Spectrophotometrical Measurements of OXPHOS Enzymes

Activities of citrate synthase and the combined activities of CII+CIII and CI+CIII were measured in cell homogenates as described previously (Birch-Machin and Turnbull, 2001).

Mouse Model of CI

Mouse CI matrix-exposed proteins were structurally aligned with the corresponding *Thermus thermofilus* homolog proteins by using the comparative modeling tool SWISS-MODEL (Bordoli and Schwede, 2012). Finally, using the Python Molecular Viewer (Sanner, 1999) we performed a manual docking of every matrix complex I protein based on the template from PDB: 2YBB of the fitted model for bovine mitochondrial SC (Althoff et al., 2011).

ROS Production and Measurement

Controlled production of ROS in cells was achieved by incubating cells for 6–8 hr in the presence of xanthine (100 μM) and xanthine oxidase (100 mU/ml). The CII inhibitor 3-nitropropionic acid (NPA) was used at 1 mM. All the reagents were purchased at Sigma-Aldrich. ROS production in control and treated fibroblasts was assessed by flow cytometry using 2,7-DCFH2-DA as the probe (Kamiński et al., 2012).

Nematode Strains and Analysis

Wild-type (*C. elegans*, N2, Bristol) and the gas-1(fc21) mutant were obtained from the Caenorhabditis Genetics Center, and growth was maintained in standard conditions (Stiernagle, 2006). Control and mutant worms were grown with 7 μM rotenone in nematode growth medium (NGM) plates (standard plates) for 10 hr at 20°C. After 10 hr, the gas-1 worms move slowly, and when the plates are very fresh, they begin to die. Wild-types (N2) looked and moved normally in these conditions (see Table S3). BNGE was performed as described previously (Pujol et al., 2013). Western blotting was performed using PVDF membranes and the iBlot system (Invitrogen). CI was detected with a 1:1,000 dilution of monoclonal anti-human NDUFS3 (the homolog of *C. elegans* NUO-2) (MS112, mouse, MitoSciences). CV was detected with a 1:1,000 dilution of monoclonal anti-ATP synthase subunit alpha (MS507, mouse, MitoSciences).

SUPPLEMENTAL INFORMATION

Supplemental Information includes Supplemental Experimental Procedures, five figures, and three tables and can be found with this article online at http://dx.doi.org/10.1016/j.celrep.2016.03.009.

ACKNOWLEDGMENTS

We thank Dr. Concepción Jimenez, Ana Latorre-Pellicer, Andrés Gonzalez-Guerra, and Marta Roche for technical assistance and Simon Bartlett for English editing. This study was supported by grants from the Ministerio de Economía y Competitividad (SAF2012-32776, BIO2012/37926, and CSD2007-00020), the Comunidad de Madrid (CAM/S2010), the EU (UE0/GA317433 and UE0/MCA1201), and the Instituto de Salud Carlos III (FIS grants PI14-01962 and PI12-01297, Redes-RD12/0042/0056, and ProteoRed-PT13/0001/0017). A.G. is the recipient of an FPI fellowship (MIN/FPI1009). C.T.M. and F.D. were supported by the NIH (grants 1R01NS079965, 1R01AG036871, and 1R01GM101225, respectively). The CNIC is supported by the Ministerio de Economía y Competitividad and the Pro-CNIC Foundation.

Received: August 27, 2015
Revised: February 3, 2016
Accepted: February 27, 2016
Published: March 24, 2016

REFERENCES

Acín-Pérez, R., Bayona-Bafaluy, M.P., Fernández-Silva, P., Moreno-Loshuertos, R., Pérez-Martos, A., Bruno, C., Moraes, C.T., and Enríquez, J.A. (2004). Respiratory complex III is required to maintain complex I in mammalian mitochondria. Mol. Cell *13*, 805–815.

Acín-Pérez, R., Fernández-Silva, P., Peleato, M.L., Pérez-Martos, A., and Enriquez, J.A. (2008). Respiratory active mitochondrial supercomplexes. Mol. Cell *32*, 529–539.

Acín-Pérez, R., Carrascoso, I., Baixauli, F., Roche-Molina, M., Latorre-Pellicer, A., Fernández-Silva, P., Mittelbrunn, M., Sánchez-Madrid, F., Pérez-Martos, A., Lowell, C.A., et al. (2014). ROS-triggered phosphorylation of complex II by Fgr kinase regulates cellular adaptation to fuel use. Cell Metab. *19*, 1020–1033.

Althoff, T., Mills, D.J., Popot, J.-L., and Kühlbrandt, W. (2011). Arrangement of electron transport chain components in bovine mitochondrial supercomplex I1III2IV1. EMBO J. *30*, 4652–4664.

Baradaran, R., Berrisford, J.M., Minhas, G.S., and Sazanov, L.A. (2013). Crystal structure of the entire respiratory complex I. Nature *494*, 443–448.

Bayona-Bafaluy, M.P., Manfredi, G., and Moraes, C.T. (2003). A chemical enucleation method for the transfer of mitochondrial DNA to rho(o) cells. Nucleic Acids Res. *31*, e98.

Birch-Machin, M.A., and Turnbull, D.M. (2001). Assaying mitochondrial respiratory complex activity in mitochondria isolated from human cells and tissues. Methods Cell Biol. *65*, 97–117.

Bordoli, L., and Schwede, T. (2012). Automated protein structure modeling with SWISS-MODEL Workspace and the Protein Model Portal. Methods Mol. Biol. *857*, 107–136.

Brea-Calvo, G., Rodríguez-Hernández, A., Fernández-Ayala, D.J.M., Navas, P., and Sánchez-Alcázar, J.A. (2006). Chemotherapy induces an increase in coenzyme Q10 levels in cancer cell lines. Free Radic. Biol. Med. *40*, 1293–1302.

Bruno, C., Santorelli, F.M., Assereto, S., Tonoli, E., Tessa, A., Traverso, M., Scapolan, S., Bado, M., Tedeschi, S., and Minetti, C. (2003). Progressive exercise intolerance associated with a new muscle-restricted nonsense mutation (G142X) in the mitochondrial cytochrome b gene. Muscle Nerve *28*, 508–511.

Chomyn, A. (1996). In vivo labeling and analysis of human mitochondrial translation products. Methods Enzymol. *264*, 197–211.

Chouchani, E.T., Pell, V.R., Gaude, E., Aksentijević, D., Sundier, S.Y., Robb, E.L., Logan, A., Nadtochiy, S.M., Ord, E.N.J., Smith, A.C., et al. (2014). Ischaemic accumulation of succinate controls reperfusion injury through mitochondrial ROS. Nature *515*, 431–435.

Cogliati, S., Frezza, C., Soriano, M.E., Varanita, T., Quintana-Cabrera, R., Corrado, M., Cipolat, S., Costa, V., Casarin, A., Gomes, L.C., et al. (2013). Mitochondrial cristae shape determines respiratory chain supercomplexes assembly and respiratory efficiency. Cell *155*, 160–171.

Danielson, S.R., Held, J.M., Oo, M., Riley, R., Gibson, B.W., and Andersen, J.K. (2011). Quantitative mapping of reversible mitochondrial Complex I cysteine oxidation in a Parkinson disease mouse model. J. Biol. Chem. *286*, 7601–7608.

Diaz, F., Fukui, H., Garcia, S., and Moraes, C.T. (2006). Cytochrome c oxidase is required for the assembly/stability of respiratory complex I in mouse fibroblasts. Mol. Cell. Biol. *26*, 4872–4881.

Dieteren, C.E.J., Koopman, W.J.H., Swarts, H.G., Peters, J.G.P., Maczuga, P., van Gemst, J.J., Masereeuw, R., Smeitink, J.A.M., Nijtmans, L.G.J., and Willems, P.H.G.M. (2012). Subunit-specific incorporation efficiency and kinetics in mitochondrial complex I homeostasis. J. Biol. Chem. *287*, 41851–41860.

Duarte, M., and Videira, A. (2009). Effects of mitochondrial complex III disruption in the respiratory chain of Neurospora crassa. Mol. Microbiol. *72*, 246–258.

Efremov, R.G., Baradaran, R., and Sazanov, L.A. (2010). The architecture of respiratory complex I. Nature *465*, 441–445.

Enríquez, J.A. (2016). Supramolecular organization of respiratory complexes. Annu. Rev. Physiol. *78*, 533–561.

Fernández-Silva, P., Acín-Pérez, R., Fernández-Vizarra, E., Pérez-Martos, A., and Enriquez, J.A. (2007). In vivo and in organello analyses of mitochondrial translation. Methods Cell Biol. *80*, 571–588.

Galkin, A., Meyer, B., Wittig, I., Karas, M., Schägger, H., Vinogradov, A., and Brandt, U. (2008). Identification of the mitochondrial ND3 subunit as a structural component involved in the active/deactive enzyme transition of respiratory complex I. J. Biol. Chem. *283*, 20907–20913.

Galkin, A., Abramov, A.Y., Frakich, N., Duchen, M.R., and Moncada, S. (2009). Lack of oxygen deactivates mitochondrial complex I: implications for ischemic injury? J. Biol. Chem. *284*, 36055–36061.

Guerrero-Castillo, S., Vázquez-Acevedo, M., González-Halphen, D., and Uribe-Carvajal, S. (2009). In Yarrowia lipolytica mitochondria, the alternative NADH dehydrogenase interacts specifically with the cytochrome complexes of the classic respiratory pathway. Biochim. Biophys. Acta *1787*, 75–85.

Hernansanz-Agustín, P., Izquierdo-Álvarez, A., Sánchez-Gómez, F.J., Ramos, E., Villa-Piña, T., Lamas, S., Bogdanova, A., and Martínez-Ruiz, A. (2014). Acute hypoxia produces a superoxide burst in cells. Free Radic. Biol. Med. *71*, 146–156.

Hirst, J. (2013). Mitochondrial complex I. Annu. Rev. Biochem. *82*, 551–575.

Hofhaus, G., and Attardi, G. (1995). Efficient selection and characterization of mutants of a human cell line which are defective in mitochondrial DNA-encoded subunits of respiratory NADH dehydrogenase. Mol. Cell. Biol. *15*, 964–974.

Kamiński, M.M., Sauer, S.W., Kamiński, M., Opp, S., Ruppert, T., Grigaravičius, P., Grudnik, P., Gröne, H.-J., Krammer, P.H., and Gülow, K. (2012). T cell activation is driven by an ADP-dependent glucokinase linking enhanced glycolysis with mitochondrial reactive oxygen species generation. Cell Rep. *2*, 1300–1315.

Koh, M.Y., and Powis, G. (2012). Passing the baton: the HIF switch. Trends Biochem. Sci. *37*, 364–372.

Krause, F., Scheckhuber, C.Q., Werner, A., Rexroth, S., Reifschneider, N.H., Dencher, N.A., and Osiewacz, H.D. (2004). Supramolecular organization of cytochrome c oxidase- and alternative oxidase-dependent respiratory chains in the filamentous fungus Podospora anserina. J. Biol. Chem. *279*, 26453–26461.

Lagendijk, J., Ubbink, J.B., and Vermaak, W.J. (1996). Measurement of the ratio between the reduced and oxidized forms of coenzyme Q10 in human plasma as a possible marker of oxidative stress. J. Lipid Res. *37*, 67–75.

Lamantea, E., Carrara, F., Mariotti, C., Morandi, L., Tiranti, V., and Zeviani, M. (2002). A novel nonsense mutation (Q352X) in the mitochondrial cytochrome b gene associated with a combined deficiency of complexes I and III. Neuromuscul. Disord. *12*, 49–52.

Lapuente-Brun, E., Moreno-Loshuertos, R., Acín-Pérez, R., Latorre-Pellicer, A., Colás, C., Balsa, E., Perales-Clemente, E., Quirós, P.M., Calvo, E., Rodríguez-Hernández, M.A., et al. (2013). Supercomplex assembly determines electron flux in the mitochondrial electron transport chain. Science *340*, 1567–1570.

Lazarou, M., McKenzie, M., Ohtake, A., Thorburn, D.R., and Ryan, M.T. (2007). Analysis of the assembly profiles for mitochondrial- and nuclear-DNA-encoded subunits into complex I. Mol. Cell. Biol. *27*, 4228–4237.

López-Ferrer, D., Ramos-Fernández, A., Martínez-Bartolomé, S., García-Ruiz, P., and Vázquez, J. (2006). Quantitative proteomics using 16O/18O labeling and linear ion trap mass spectrometry. Proteomics *6* (*Suppl 1*), S4–S11.

Maas, M.F.P.M., Krause, F., Dencher, N.A., and Sainsard-Chanet, A. (2009). Respiratory complexes III and IV are not essential for the assembly/stability of complex I in fungi. J. Mol. Biol. *387*, 259–269.

Martínez-Acedo, P., Núñez, E., Gómez, F.J.S., Moreno, M., Ramos, E., Izquierdo-Álvarez, A., Miró-Casas, E., Mesa, R., Rodriguez, P., Martínez-Ruiz, A., et al. (2012). A novel strategy for global analysis of the dynamic thiol redox proteome. Mol. Cell. Proteomics *11*, 800–813.

Murphy, M.P. (2009). How mitochondria produce reactive oxygen species. Biochem. J. *417*, 1–13.

Naldini, L., Blömer, U., Gage, F.H., Trono, D., and Verma, I.M. (1996). Efficient transfer, integration, and sustained long-term expression of the transgene in adult rat brains injected with a lentiviral vector. Proc. Natl. Acad. Sci. USA *93*, 11382–11388.

Nath, A.K., Ryu, J.H., Jin, Y.N., Roberts, L.D., Dejam, A., Gerszten, R.E., and Peterson, R.T. (2015). PTPMT1 inhibition lowers glucose through succinate dehydrogenase phosphorylation. Cell Rep. *10*, 694–701.

Navarro, P., and Vázquez, J. (2009). A refined method to calculate false discovery rates for peptide identification using decoy databases. J. Proteome Res. *8*, 1792–1796.

Pagliarini, D.J., Calvo, S.E., Chang, B., Sheth, S.A., Vafai, S.B., Ong, S.-E., Walford, G.A., Sugiana, C., Boneh, A., Chen, W.K., et al. (2008). A mitochondrial protein compendium elucidates complex I disease biology. Cell *134*, 112–123.

Perales-Clemente, E., Bayona-Bafaluy, M.P., Pérez-Martos, A., Barrientos, A., Fernández-Silva, P., and Enriquez, J.A. (2008). Restoration of electron transport without proton pumping in mammalian mitochondria. Proc. Natl. Acad. Sci. USA *105*, 18735–18739.

Pujol, C., Bratić-Hench, I., Sumakovic, M., Hench, J., Mourier, A., Baumann, L., Pavlenko, V., and Trifunovic, A. (2013). Succinate dehydrogenase upregulation destabilize complex I and limits the lifespan of gas-1 mutant. PLoS ONE *8*, e59493.

Ramos-Fernández, A., López-Ferrer, D., and Vázquez, J. (2007). Improved method for differential expression proteomics using trypsin-catalyzed 18O labeling with a correction for labeling efficiency. Mol. Cell. Proteomics *6*, 1274–1286.

Sanner, M.F. (1999). Python: a programming language for software integration and development. J. Mol. Graph. Model. *17*, 57–61.

Schägger, H., and Pfeiffer, K. (2000). Supercomplexes in the respiratory chains of yeast and mammalian mitochondria. EMBO J. *19*, 1777–1783.

Sheftel, A.D., Stehling, O., Pierik, A.J., Netz, D.J.A., Kerscher, S., Elsässer, H.-P., Wittig, I., Balk, J., Brandt, U., and Lill, R. (2009). Human ind1, an iron-sulfur cluster assembly factor for respiratory complex I. Mol. Cell. Biol. *29*, 6059–6073.

Speijer, D. (2011). Oxygen radicals shaping evolution: why fatty acid catabolism leads to peroxisomes while neurons do without it: $FADH_2$/NADH flux ratios determining mitochondrial radical formation were crucial for the eukaryotic invention of peroxisomes and catabolic tissue differentiation. BioEssays *33*, 88–94.

Stiernagle, T. (2006). Maintenance of C. elegans. WormBook *11*, 1–11.

Szklarczyk, R., Wanschers, B.F.J., Nabuurs, S.B., Nouws, J., Nijtmans, L.G., and Huynen, M.A. (2011). NDUFB7 and NDUFA8 are located at the intermembrane surface of complex I. FEBS Lett. *585*, 737–743.

Ten, V.S., and Starkov, A. (2012). Hypoxic-ischemic injury in the developing brain: the role of reactive oxygen species originating in mitochondria. Neurol. Res. Int. *2012*, 542976.

Vempati, U.D., Han, X., and Moraes, C.T. (2009). Lack of cytochrome c in mouse fibroblasts disrupts assembly/stability of respiratory complexes I and IV. J. Biol. Chem. *284*, 4383–4391.

Vinothkumar, K.R., Zhu, J., and Hirst, J. (2014). Architecture of mammalian respiratory complex I. Nature *515*, 80–84.

Wittig, I., Braun, H.-P., and Schägger, H. (2006). Blue native PAGE. Nat. Protoc. *1*, 418–428.

Cell Reports, Volume *15*

Supplemental Information

The CoQH2/CoQ Ratio Serves as a Sensor of Respiratory Chain Efficiency

Adela Guarás, Ester Perales-Clemente, Enrique Calvo, Rebeca Acín-Pérez, Marta Loureiro-Lopez, Claire Pujol, Isabel Martínez-Carrascoso, Estefanía Nuñez, Fernando García-Marqués, María Angeles Rodríguez-Hernández, Ana Cortés, Francisca Diaz, Acisclo Pérez-Martos, Carlos T. Moraes, Patricio Fernández-Silva, Aleksandra Trifunovic, Plácido Navas, Jesús Vazquez, and Jose A. Enríquez

SUPPLEMENTARY MATERIAL FOR:

The CoQH2/CoQ ratio serves as a sensor of respiratory chain efficiency

Adela Guarás[1], Ester Perales-Clemente [1], Enrique Calvo[2], Rebeca Acín-Pérez[1], Marta Loureiro-López[2], Claire Pujol[3], Isabel Martínez-Carrascoso[1], Estefanía Nuñez[2], Fernando García-Marqués[2], M. A. Rodríguez-Hernández[4], Ana Cortés, Francisca Diaz[5], Acisclo Pérez-Martos[7], Carlos T. Moraes[5,6], Patricio Fernández-Silva[7], Aleksandra Trifunovic[3], Plácido Navas[4], Jesús Vazquez[2] and J.A. Enríquez[1,7*]

INVENTORY:

Detailed description of the proteomic methodology:

Mitochondrial proteomics by data-independent scanning (DiS) mass spectrometry. Mitochondrial Cys-thiol redox status was studied by the GELSILOX method (Martínez-Acedo et al., 2012). The resulting tryptic peptide mixtures were subjected to nano-liquid chromatography coupled to mass spectrometry using a data-independent scanning (DiS) method. Peptides were injected onto a C-18 reversed phase (RP) nano-column (75 mm I.D. and 50 cm, Acclaim PepMap, Thermo Fisher, San José, CA, USA) and analyzed in a continuous acetonitrile gradient consisting of 8-31% B for 130 min, 50-90% B for 1 min (B=0.5% formic acid in acetonitrile). Peptides were eluted from the RP nano-column at a flow rate of ~200 nL/min to an emitter nanospray needle for real-time ionization and peptide fragmentation in a Q-Exactive mass spectrometer (Thermo Fisher). Each sample was analyzed in two chromatographic runs covering different mass ranges (from 400 to 750 Da and from 750 to 1100 Da). The DiS cycle consisted of 175 sequential HCD MS/MS fragmentation events with 2 Da-windows that covered each whole 350 Da-range. HCD fragmentation was performed at a resolution of 17,500 and a maximum injection time of 80 ms with the AGC set to a target of $3x10^5$ ions. The whole cycle lasted 30 seconds or less depending on ion intensity during chromatography. The narrow windows used for fragmentation allowed peptide identification using conventional shotgun searching algorithms. This was done using Sequest running under Proteome Discoverer 1.4.0.288 (Thermo Fisher Scientific), allowing two missed cleavages, and using 2 Da and 10 ppm precursor and fragment mass tolerances, respectively. Met oxidation and Cys carbamydomethylation or methylthiolation were selected as dynamic modifications. 1% FDR was used as a criterion for peptide identification; this parameter was estimated using a separate inverted database (Navarro and Vázquez, 2009). Semiquantitative monitorization of identified peptides was performed in the MS/MS spectra using Sequest's SpScore.

Quantitative analysis of mitochondrial proteins. After in-gel trypsin digestion, all the reoxygenation samples were equally mixed with a control sample (hypoxia) labeled with ^{18}O. Peptide quantification from FullScan spectra and labeling efficiency calculation were performed as described (López-Ferrer et al., 2006; Ramos-Fernández et al., 2007), using QuiXoT, a program written in C# in our laboratory. Data statistical analysis was done on the basis of a recently developed and validated random-effects model that includes four different sources of variance: at the spectrum-fitting, scan, peptide and protein levels (Jorge et al., 2009). Briefly, the standardized variable zq describes the log2 ratio for each protein corrected for the corresponding systematical error, in each experiment.

Legends to supplementary figures:

Supplementary Figure 1.- AOX does not interact physically with complex I. Related to Figure 1. A, AOX expression and subcellular localization in $CYTB^{KO}$AOX, $Cox10^{KO}$AOX and $CYTC^{KO}$AOX cells. AOX was immunodetected with anti-HA and mitochondrial localization was confirmed by colocalization with MitoTracker red. **B,** Complex I was immunoprecipitated from digitonin-solubilized mitochondria of $CYTB^{KO}$ cells and isogenic controls expressing AOX ($CYTB^{KO}$AOX and C57AOX). Lysates (not bound) and immunoprecipitates (IPCI) were probed with anti-NDUFB6 (complex I), anti-Fp (70 kDa complex II), anti-Core2 (complex III) and anti-COI (complex IV). VDAC, Tom20 and prohibitin were immunodetected as mitochondrial markers. AOX was detected with anti-HA (AOXHA). A long exposure of the AOX blot is shown on the left.

Supplementary Figure 2.- Detailed Effect of AOX on CI Subunits. Related to Figure 2. 1D and 2D blue-native electrophoresis of [^{35}S]-methionine pulse-labeled mtDNA-encoded proteins from control cells (C_B, C_{10} & C_C), mutant cells (Cytb^{KO}, Cox10^{KO} & Cytc^{KO}) or mutant cells expressing AOX (Cytb^{KO}AOX, Cox10^{KO}AOX & Cytc^{KO}AOX). ND6, ND5, ND4, ND4L, ND3, ND2 and ND1 are subunits 1, 2, 3, 4, 5 and 6 of CI. COI, COII, and COIII are subunits 1, 2 and 3 of CIV. cyt b is the cytochrome b subunit of CIII. A6 and A8 are subunits of complex V.

Supplementary Figure 3.- Complex I stabilization in Cox10^{KO} cells is HIF-1α-independent. Related to Figure 4. **A,** Hypoxia does not alter the $CoQH_2$/CoQ ratio. Percentage of reduced CoQ in Cox10^{KO} cells grown in normoxia and after switching to 1% hypoxia. Data are means ± SD n=3. **B,** Quantitative RT-PCR analysis of mRNA expression of the known HIF-1α target genes prolyl hydroxylase domain protein 3 (*Phd3*) and pyruvate dehydrogenase kinase isoenzyme 1 (*Pdk1*) as positive controls for HIF-1α stabilization. Analysis was conducted in control cells (C_{10}) and mutant cells (Cox10^{KO}) grown at 21% O_2 or 1% O_2 and treated with vehicle (DMSO) or DMOG (0.5 mM) for 72 hours and after culture at 21% O_2 without treatment (n≥ 3. mean ± SEM; *p<0.05; Wilcoxon test). **C,** Blue native electrophoresis and western blot of digitonin-solubilized mitochondrial proteins from wild type cells (C_{10}) or cells lacking CIV (Cox10^{KO}) grown under different conditions.

Supplementary Figure 4.- GELSILOX-targeted proteomics. Related to Figure 5. **A,** Quantification of CI proteins as a proportion of total mitochondrial proteins (assembled and not assembled) assessed as the number of identified complex-I-derived peptides at each reoxygenation time, relative to hypoxia (no reoxygenation; 100%). **B,** ^{18}O-labeling analysis of proteins belonging to complexes II to V during reoxygenation. **C,** Relative proportions of oxidized vs. reduced Cys-containing peptides identified in the total mitochondrial proteome (ALL) or in the indicated respiratory complex (CI, CII, CIII) obtained using the GELSILOX technique. **D,** Representative example of time monitoring of SpScores during chromatography runs for the GELSILOX-reacted Cys-containing peptide NACGSDYDFDVFVVR, from the complex I protein NDUFV1. **E,** Representative example of HCD fragmentation spectra for the oxidized and reduced species. Main fragments from the y-carboxy series are marked.

Supplementary Figure 5.- Physiological relevance of RET. Related to Figure 6. **A,** Densitometry traces of the electrophoretic bands in the gel shown in Figure 6A, illustrating the decrease in CI induced by the fuel shift from glucose to fatty acids but not to galactose. The decrease was evident in all three bands containing CI. These cells are unable to incorporate CIV into supercomplexes due to the lack of SCAFI (Lapuente-Brun et al., 2013). **B,** Densitometry traces of the electrophoretic bands in the gel shown in Figure 6B (SCAFI wild-type), illustrating the decrease in CI induced by the fuel shift from glucose to fatty acids, mainly affecting SCI+III^{SL} and SCI+III+IV. In this case the shift from glucose to galactose exerts the opposite effect, inducing a general increase in of CI in all bands. **C, D**, Box plot presenting the impact of Fgr tyrosine kinase ablation and SDHA Y604F mutation on H_2O_2-triggered CII and CI activities.

Supplementary Table 1. - Total amount of CoQ (red + ox) in the different cell lines used in this study.

Cell type	CoQ9 (pmol/mg prot)+SD
C_b	133.29±16 (n=6)
$Cytb^{KO}$	172.67±24 (n=6)
$Cytb^{KO}$+AOX	143.31±17 (n=6)
C_{10}	165.57± 21(n=5)
$Cox10^{KO}$	186.50±29 (n=5)
$Cox10^{KO}$+AOX	166.05±15 (n=5)
C_c	170.81±31 (n=3)
$Cytc^{KO}$	197.62± 35 (n=3)
$Cytc^{KO}$+AOX	176.07±23 (n=3)

Supplementary Table 2. - Oxidative changes observed in complex I cysteines in two models of oxidative stress

	Cysteine	Peptide	*Thermus thermophilus*	Reoxygenation[a]		Glutathione depletion[b]		Potential role[c]
				Detected	Cys oxidation	Detected	Cys oxidation	
Ndufs1	75	LSVAGNcR	Nqo3-Cys45	Yes	No	Yes	No	I-S cluster
	78	McLVEIEK	Nqo3- Cys48	Yes	Yes	Yes	No	I-S cluster
	92	VVAAcAMPVMK	Nqo3- Cys83	Yes	Yes	Yes	Yes	I-S cluster
	176/179	cIQcTR	Nqo3-Cys181/184	Yes	No	No	-	I-S cluster
	463	HSFcEVLK	Nqo3- Lys494	Yes	Yes	Yes	Yes	Unknown
	554	MLFLLGADGGcITR	Nqo3- Val571	Yes	Yes	Yes	No	Unknown
Ndufv1*	125	YLVVNADEGEPGTcK	Nqo1-Phe101	Yes	Yes	Yes	No	Unknown
	142	LVEGcLVGGR	Nqo1-Met118	Yes	Yes	Yes	No	Unknown
	187	NAcGSDYDFDVFVVR	Nqo1-Phe163	Yes	Yes	No	-	Unknown
Ndufs2	347	IIEQcLNK	Nqo4-Ala293	Yes	Yes	Yes	Yes	Unknown
Nd3	39	ANPYEcGFDPTSSAR	Nqo7-Ala39	Yes	Yes	Yes	No	CI activation

[a]Re-oxygenation, data obtained in this report. [b]Glutathione depletion (Danielson et al., 2011). [c]The potential role of each cysteine is inferred by homology with *Thermus thermophilus*. The sequences for alignment were obtained in Uniprot (Uniprot subunit ID: Ndufs1/Q91VD9, Ndufv1/Q91YT0, Ndufs2/Q91WD5, Nd3/P03899, Nqo3/Q56223, Nqo1/Q56222, Nqo4/Q56220, Nqo7/Q56217).

The table compares our analysis with a recent reported quantitative map of mitochondrial CI cysteine oxidation in brain mitochondria upon glutathione depletion (Danielson et al., 2011). This report showed that NDUFS1 (Cys^{92}, Cys^{463} & Cys^{554}) and NDUFS2 (Cys^{347}) cysteines were among the more sensitive to oxidation. Notably two of these cysteines match those that we identified, and Cys^{92} in NDUFS1 belongs to the iron-sulfur cluster in which we detected Cys^{75} and Cys^{78}. In agreement with our findings, the report showed that cysteines in NDUFB7 and NDUFA8 have a high basal level of oxidation, but contrary to our data, the reported glutathione depletion model did not detect significant alteration in the cysteine oxidation status of NDUFV1(Danielson et al., 2011). This may indicate a fundamental difference in the mechanism of oxidative stress between the two models. Glutathione depletion reduces ROS scavenging capacity and would not increase ROS production by CI. RET would induce ROS production in CI. The fact that NDUFV1, the CI subunit that holds the flavin co-factor, appears to be very sensitive to oxidization in our conditions is also in agreement with the proposal that CI superoxide is produced by the reduction of the flavin in both forward electron transport (FET) and RET(Pryde and Hirst, 2011).

Supplementary Table 3.- Response of gas-1 *C. elegans* mutant to rotenone.

		Time (hours)					
Tª	Conc Rotenone	0	5	7	10	12	24
20°C	25 µM	10	1	0	0	0	0
	10 µM	20	18	16	14	12	3
	5 µM	10	9	9	9	8	5
	1 µM	5	5	5	4	4	4
25°C	25 µM	10	0	0	0	0	0
	10 µM	20	17	15	12	8	3
	5 µM	10	10	7	6	6	1
	1 µM	5	5	5	5	5	4

Figures indicate number of live gas-1 worms at the indicated rotenone doses and growing temperature. Wild-type worms were in all cases insensitive to the treatment.

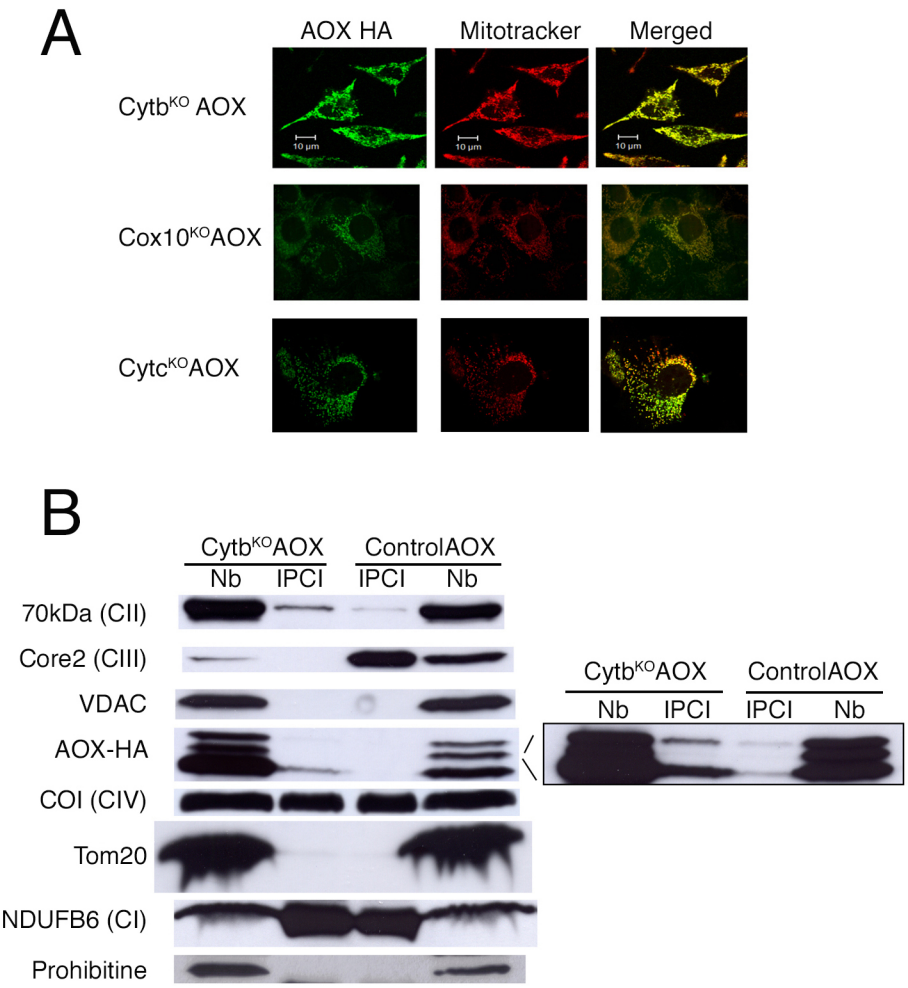

Supplementary Figure 1

Supplementary Figure 2

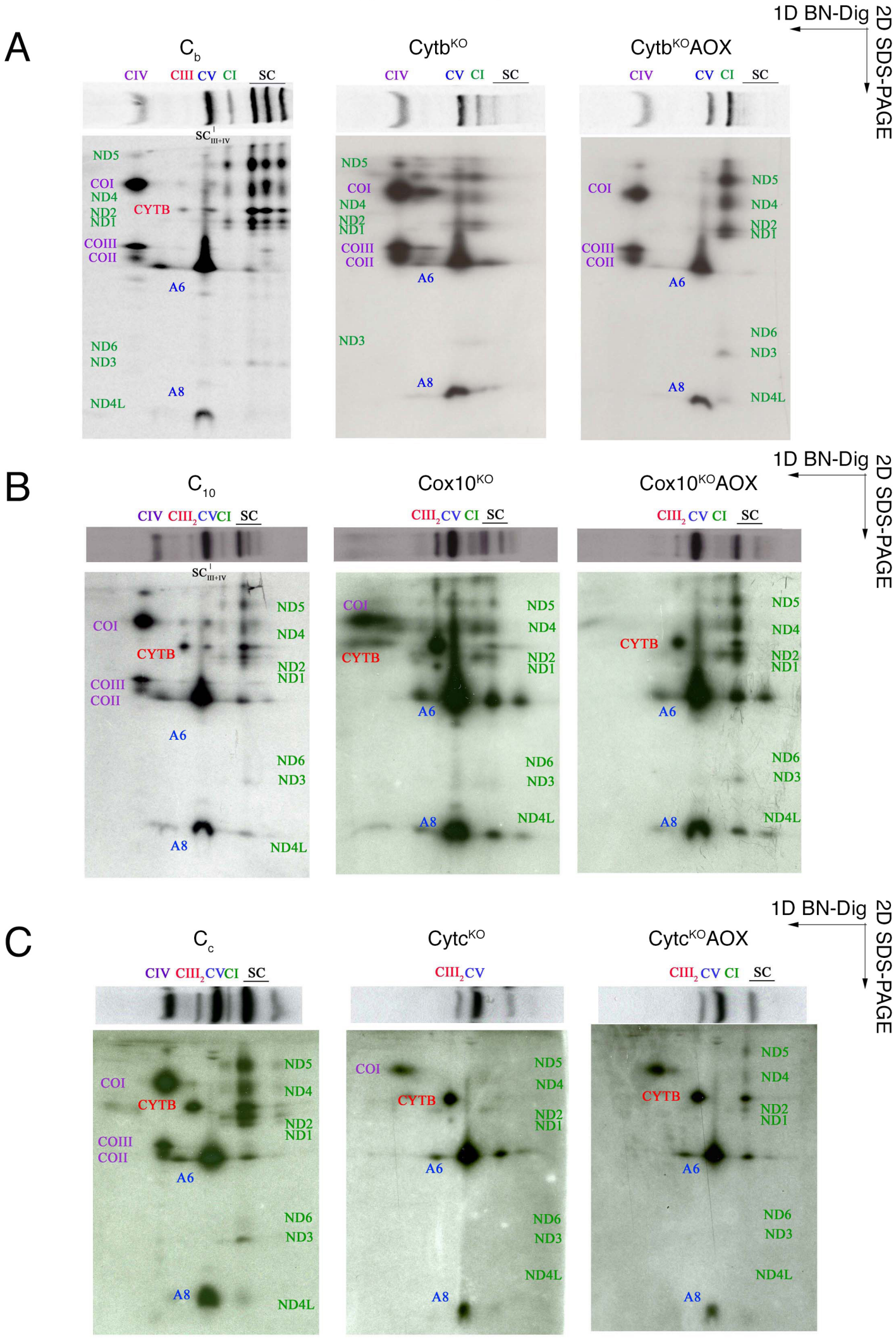

Supplementary figure 3

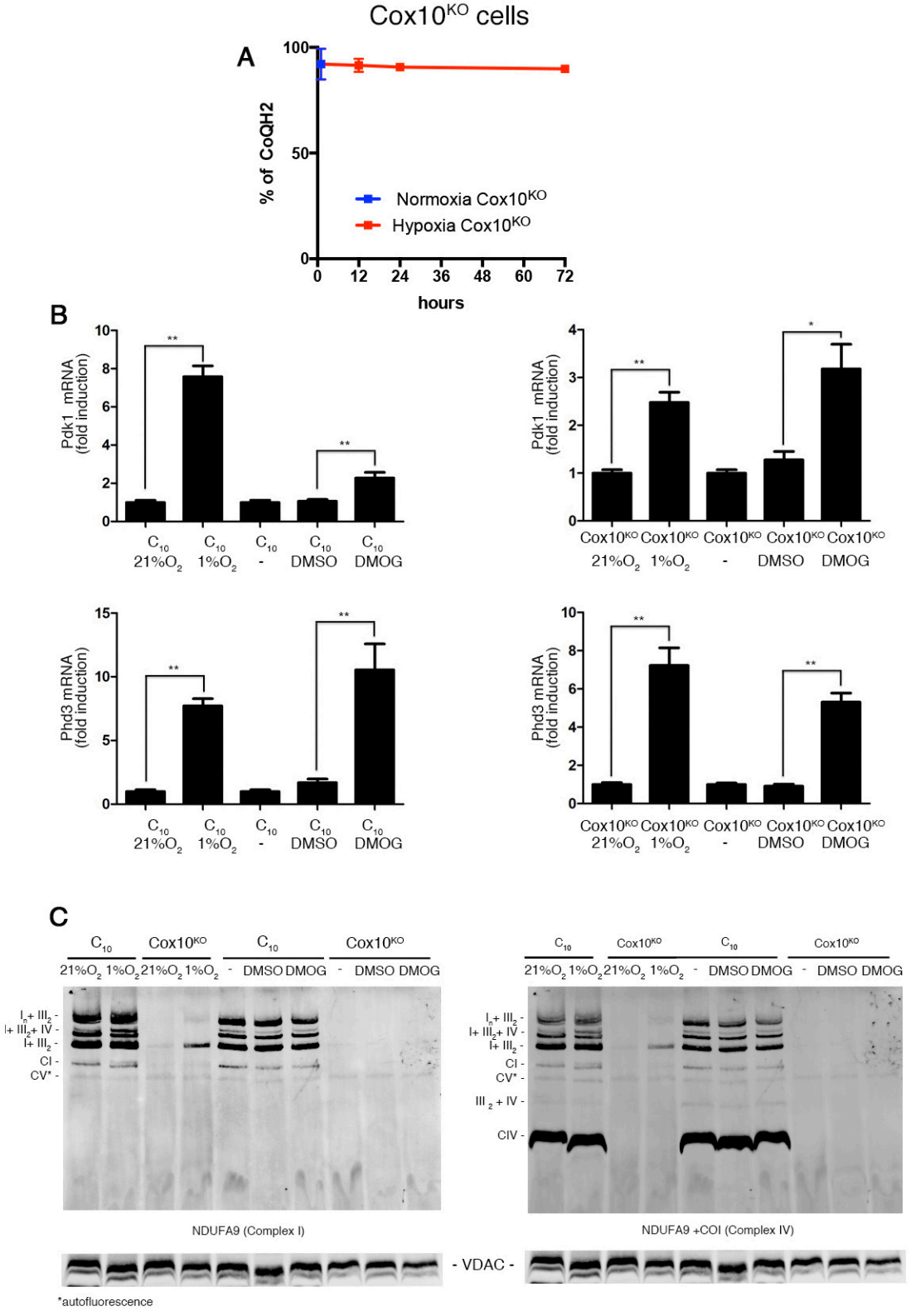

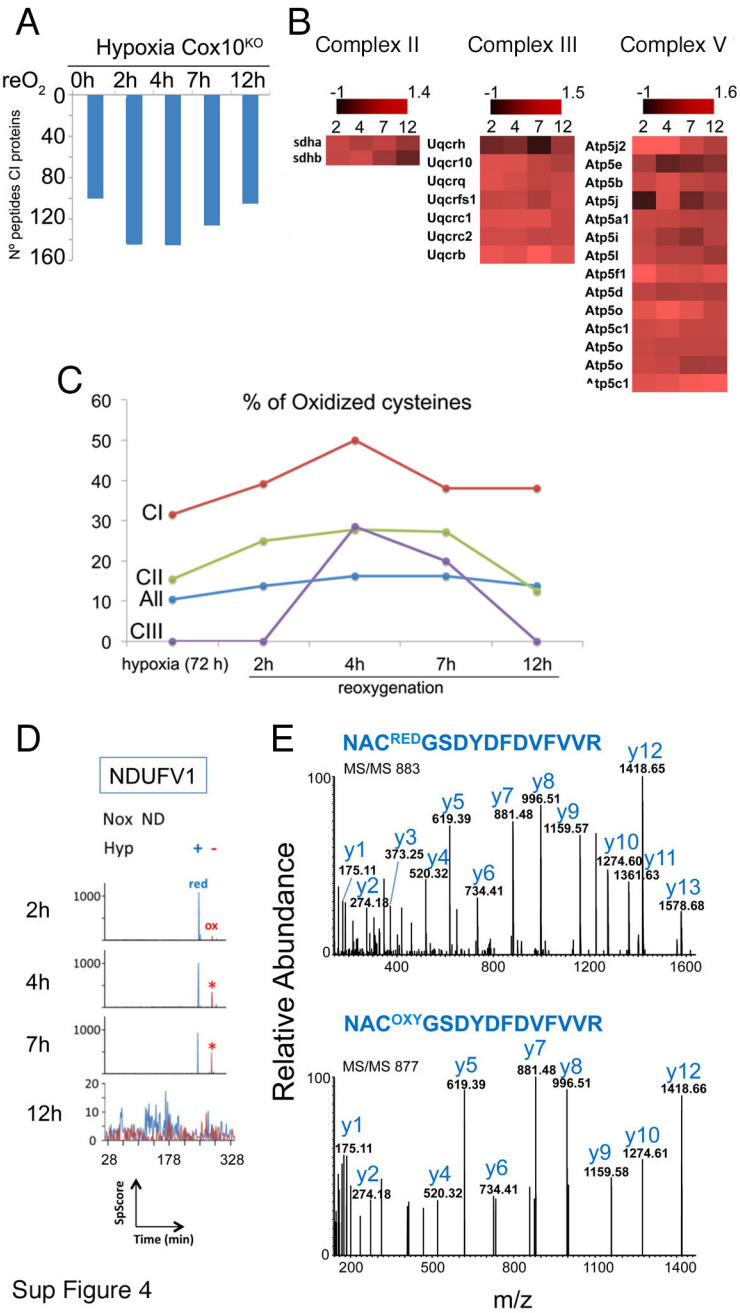
A
Hypoxia Cox10KO
reO2
0h 2h 4h 7h 12h
Nº peptides CI proteins
0
40
80
120
160
B
Complex II
Complex III
Complex V
-1 1.4
2 4 7 12
sdha
sdhb
-1 1.5
Uqcrh
Uqcr10
Uqcrq
Uqcrfs1
Uqcrc1
Uqcrc2
Uqcrb
-1 1.6
Atp5j2
Atp5e
Atp5b
Atp5j
Atp5a1
Atp5i
Atp5l
Atp5f1
Atp5d
Atp5o
Atp5c1
Atp5o
Atp5o
^tp5c1
C
% of Oxidized cysteines
CI
CII
AII
CIII
hypoxia (72 h)
2h
4h
7h
12h
reoxygenation
D
NDUFV1
Nox ND
Hyp + -
red
ox
2h
4h
7h
12h
SpScore
Time (min)
E
NACREDGSDYDFDVFVVR
MS/MS 883
NACOXYGSDYDFDVFVVR
MS/MS 877
Relative Abundance
m/z

Sup Figure 4

Supplementary figure 5